Dear Author:

Please find attached the final pdf file of your contribution, which can be viewed using the Acrobat Reader, version 3.0 or higher. We would kindly like to draw your attention to the fact that copyright law is also valid for electronic products. This means especially that:

- You may not alter the pdf file, as changes to the published contribution are prohibited by copyright law.

- You may print the file and distribute it amongst your colleagues in the scientific community for scientific and/or personal use.

- You may make your article published by Springer-Verlag available on your personal home page provided the source of the published article is cited and Springer-Verlag is mentioned as copyright holder. You are requested to create a link to the published article in Springer's internet service. The link must be accompanied by the following text: The original publication is available at http://link.springer.de or at http://link.springer-ny.com . Please use the appropriate URL and/or DOI for the article. Articles disseminated via SpringerLink are indexed, abstracted and referenced by many abstracting and information services, bibliographic networks, subscription agencies, library networks and consortia.

- Without having asked Springer-Verlag for a separate permission your institute/your company is not allowed to place this file on its homepage.

- Please address any queries to the production editor of the journal in question, giving your name, the journal title, volume and first page number.

Yours sincerely,

Springer-Verlag

S. P. Harrison · J. E. Kutzbach · Z. Liu
P. J. Bartlein · B. Otto-Bliesner · D. Muhs
I. C. Prentice · R. S. Thompson

Mid-Holocene climates of the Americas: a dynamical response to changed seasonality

Abstract Simulations of the climatic response to mid-Holocene (6 ka BP) orbital forcing with two coupled ocean–atmosphere models (FOAM and CSM) show enhancement of monsoonal precipitation in parts of the American Southwest, Central America and northernmost South America during Northern Hemisphere summer. The enhanced onshore flow that brings precipitation into Central America is caused by a northward displacement of the inter-tropical convergence zone, driven by cooling of the equatorial and warming of the northern subtropical and mid-latitude ocean. Ocean feedbacks also enhance precipitation over the American Southwest, although the increase in monsoon precipitation there is largely driven by increases in land-surface temperature. The northward shift in the equatorial precipitation band that causes enhanced precipitation in Central America and the American Southwest has a negative feedback effect on monsoonal precipitation in northern South America. The simulations demonstrate that mid-Holocene aridity in the mid-continent of North America is dynamically linked to the orbitally induced enhancement of the summer monsoon in the American Southwest, with a spatial structure (wet in the Southwest and dry in the mid-continent) similar to that found in strong monsoon years today. Changes in winter precipitation along the west coast of North America, in Central America and along the Gulf Coast, caused by southward-displacement of the westerly storm tracks, indicate that changes in the Northern Hemisphere winter monsoon also play a role in regional climate changes during the mid-Holocene. Although the simulations with FOAM and CSM differ in detail, the general mechanisms and patterns are common to both. The model results thus provide a coherent dynamical explanation for regional patterns of increased or decreased aridity shown by vegetation, lake status and aeolian data from the Americas.

S. P. Harrison (✉) · I. C. Prentice
Max Planck Institute for Biogeochemistry,
PO Box 100164, 07701 Jena, Germany
E-mail: sharris@bgc-jena.mpg.de

J. E. Kutzbach · Z. Liu
Center for Climatic Research,
University of Wisconsin-Madison, 1225 West Dayton Street,
Madison, WI 53706, USA

P. J. Bartlein
Department of Geography, University of Oregon,
Eugene, Oregon, OR 97403-1251, USA

B. Otto-Bliesner
National Center for Atmospheric Research,
PO Box 3000, Boulder, CO 80307, USA

D. Muhs · R. S. Thompson
U.S. Geological Survey,
Earth Surface Processes Team, Box 25046,
MS980, Denver, CO 80225, USA

1 Introduction

The climates of all the continents have monsoonal characteristics, in the sense that seasonal changes in insolation cause larger changes of temperature over land than over the ocean because of the lower thermal inertia of land compared to ocean; in summer this differential heating sets up a direct thermal circulation pattern with upward vertical motion over the continents, low-level advection of moisture from ocean to land, and upper-level return flow from land to ocean (see Webster 1987). Monsoonal features are most evident in the largest continents, such as Asia, but are also apparent in the

Americas (see e.g., Tang and Reiter 1984; Douglas et al. 1993; Adams and Comrie 1997; Zhou and Lau 1998). It is therefore to be expected that changes in insolation, such as occurred in the mid-Holocene due to changes in Earth's orbital parameters, should cause changes in the monsoonal characteristics of climate. Such monsoonal changes have indeed been simulated with climate models (Kutzbach and Otto-Bliesner 1982). However, analyses of these simulations have tended to focus on the large monsoonal changes in Africa and Asia (see e.g., Joussaume et al. 1999). As part of a systematic analysis of mid-Holocene monsoon changes world-wide (Liu et al. unpublished), we focus here on changes over the Americas.

Analyses of palaeoenvironmental data have shown that parts of southwestern North America experienced greater-than-present precipitation during the mid-Holocene in response to changes in orbital forcing (Thompson et al. 1993; Mock and Brunelle-Daines 1999). Increased precipitation also occurred further south, in Mexico, Central America and the northwestern part of South America (Metcalfe et al. 2000; Markgraf et al. 2000). Coincident with this monsoon enhancement in the southwest, the mid-continent experienced drier-than-present conditions (Ritchie and Harrison 1993; Thompson et al. 1993; Webb et al. 1993; Mock and Brunelle-Daines 1999; Muhs and Zárate 2001; Forman et al. 2001). The mid-continent drying was tentatively attributed to increased summertime evaporation (caused by the summertime increase of insolation) that exceeded any increase of precipitation (see e.g., Kutzbach and Webb 1993). However, this explanation now appears unconvincing, in part because data sets from central Eurasia do not indicate general mid-continental drying in the mid-Holocene (Harrison et al. 1996, 1998; Prentice et al. 2000).

A satisfactory explanation for the observed pattern of mid-Holocene climate changes in North America requires a dynamically consistent explanation for the simultaneous occurrence of wetter and drier regimes, and their spatial pattern. Recent studies of the natural variability of the modern southwest North American monsoon have shown that enhanced precipitation in the southwest is associated with relatively drier conditions in surrounding areas due to increased subsidence in these surrounding areas (Higgins et al. 1997, 1998; Higgins and Shi 2000). Here, we use climate model simulations for the mid-Holocene to demonstrate that this wet/dry spatial pattern of interannual variability had a counterpart in the mid-Holocene, when the increase in summertime insolation produced enhanced monsoons in the American Southwest but drier-than-present conditions elsewhere. The simulated patterns are in reasonable agreement with the mid-Holocene pattern of moisture changes in the Americas. Thus, we propose that a combination of thermal and dynamical responses to mid-Holocene orbital forcing explains the regional patterns of changes in aridity shown by mid-Holocene palaeodata. We also use climate simulations with and without coupled ocean dynamics to identify the relative importance of ocean feedback processes compared to the more direct effects of insolation changes over the continent.

2 Modern climatology

2.1 Monsoonal aspects of American climates

Some large-scale features of the modern climate are direct responses to the seasonal cycle of solar radiation. These responses are monsoonal, in the sense that a strong linkage exists between the seasonal insolation cycle, land–ocean temperature differences, the large-scale circulation of the atmosphere and ocean, and, in particular, the occurrence of strong summer and winter precipitation maxima. For example, in response to the Northern Hemisphere summer insolation maximum, the Northern Hemisphere American continents warm, and the region from the equator northward through Central America and into the northern mid-latitudes has a summer precipitation maximum (Fig. 1b). The only exceptions to this pattern are relatively small areas that experience a winter maximum (or both winter and summer maxima) in parts of the west and northeast, and areas that experience a spring maximum in the west and southeast. The timing of the precipitation maximum serves to define the region strongly influenced by the Northern Hemisphere American summer monsoon.

The North American summer monsoon (Bryson and Lowrie 1955; Tang and Reiter 1984; Adams and Comrie 1997), the Mexican monsoon (Douglas et al. 1993) and the South American monsoon (Zhou and Lau 1998) do not fit exactly the definitions of monsoons that are commonly applied to the large African/Asian continents (e.g., Ramage 1971; Webster 1987). However, they operate in response to mechanisms very similar to those of the Asian monsoon, including heating on the Colorado Plateau, the Central American highlands and the high Bolivian Plateau and concomitant focusing of precipitation. The climatology of 200 mb velocity potential (not shown) shows divergent outflow from the Amazon Basin in DJF, and divergent outflow from northern South America and the American Southwest in summer (June–July–August: JJA) (see e.g., Rasmusson and Arkin 1993). These patterns of summertime upper-troposphere divergences, while weaker than their Asian counterparts, are also a dynamical index of monsoonal processes in the Americas. Although the precipitation over North America has a strong seasonal character, the absolute amount of summertime precipitation associated with the North American monsoon is substantially less than the precipitation associated with the South American summer monsoon in the Amazon Basin (December–January–February: DJF) (Fig. 1a), or with the monsoons of India and East Asia (Fein and Stephens 1987; Liu et al. unpublished).

In response to the wintertime insolation minimum, the North American continent cools markedly and the
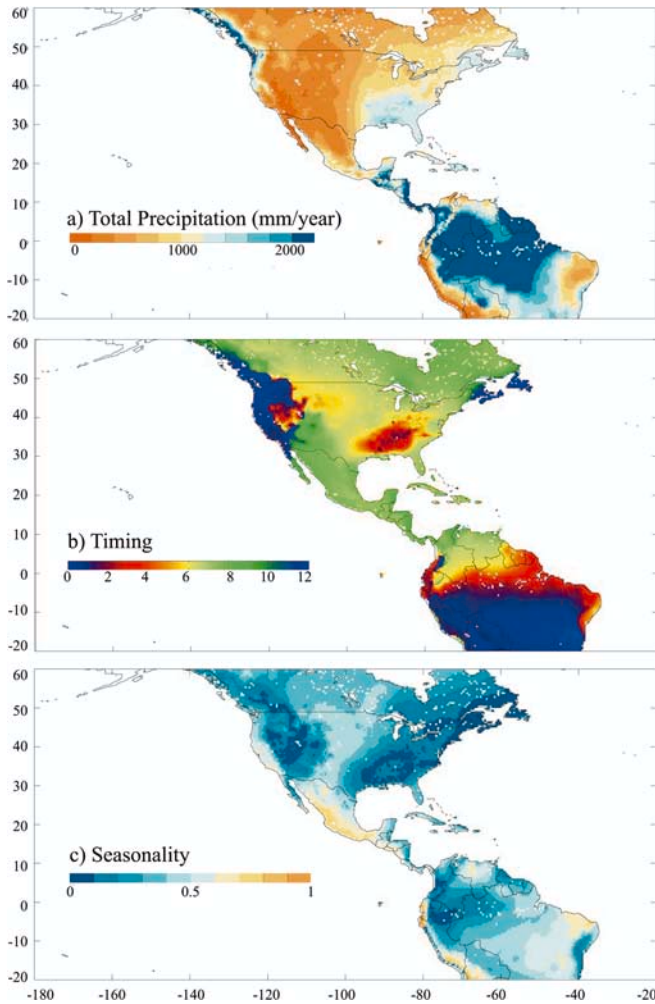
Fig. 1 Modern climatological precipitation patterns across America: **a** total precipitation, **b** the timing of maximum precipitation, and **c** seasonality of precipitation. To calculate timing and seasonality, the monthly data are represented as vectors whose direction represents the Julian day corresponding to the middle of the month ($2\pi = 365$ days). Timing is defined as the direction of the mean precipitation vector and seasonality is proportional to its length. In **b** 0 represents January 1 and 12 represents December 31. In **c** 0 represents annually uniform precipitation, 1 represents concentration of precipitation in a single month. The value 0.5 implies that rain occurs in 6 months of the year, but these months do not have to be contiguous. The data are derived from the CLIMATE 2.2 data set (http://www.pik-potsdam.de/~cramer/climate.htm) of long-term mean monthly precipitation totals

climatological location of the storm track shifts southward. Over the eastern two thirds of the continent, the prevailing wind direction switches from south in summer (June–July–August: JJA) to north in winter (December–January–February: DJF). These changes in temperature, storm tracks, and prevailing wind direction are manifestations of the Northern Hemisphere American winter monsoon, and account for winter precipitation maxima along the west coast of North America (Fig. 1b). Simultaneously, South America south of the equator experiences a strong austral-summer precipitation maximum (Fig. 1b).

2.2 Regional pattern of modern interannual variability associated with the Southwest monsoon

In addition to the direct response of American Southwest monsoon precipitation to the normal seasonal insolation cycle, it has been shown that dynamical processes associated with internanual variability cause "remote" responses as well. Studies of interannual variability can reveal natural modes of behaviour that can also be excited by changes in external forcing. For example, composite maps for summers with enhanced monsoonal precipitation over Arizona show relatively drier conditions in the Pacific Northwest, the northern Great Plains, and the mid-continent due to the formation of a crescent-shaped region of enhanced subsidence bordering the area of the enhanced monsoon (Higgins et al. 1997, 1998; Higgins and Shi 2000).

A plausible explanation for this crescent-shaped feature has been described by Rodwell and Hoskins (2001). They suggest that the inflow to the monsoon core from this crescent-shaped region has a downward-directed component (moving along the isentropic surfaces that slope downwards towards the warm Southwest); this sinking motion may be further enhanced by increased diabatic cooling in the drier air. The Great Plains and the mid-continent still experience a summer precipitation maximum, but the magnitude of the maximum is reduced in those summers when monsoonal precipitation in Arizona is stronger than normal. The patterns shown by Higgins et al. (1997) are apparent using gridded NCEP reanalysis data (Kistler et al. 2001) and station data from the GHCN network (Peterson and Vose 1999) (Fig. 2). The NCEP reanalysis data and the GHCN data show that summers (JJA) when the Arizona monsoon is strong are characterised by wetter-than-average conditions in a region stretching from Central America into the southwestern United States. This wetter-than-normal region is surrounded by a drier-than-normal region that extends from the Pacific Northwest across the Great Plains and into the Mississippi Valley. The NCEP and GHCN data show a pattern opposite in sign in years when monsoonal precipitation over Arizona and New Mexico is less than normal. The NCEP reanalysis data indicates that the crescent of decreased precipitation around the monsoon core regions during strong-monsoon years is related to stronger-than-normal subsidence in this region (shown by positive, i.e., greater sinking, 500 mb vertical velocity or "omega" anomalies: Fig. 2). In contrast, during weak-monsoon years, the core monsoon region shows weaker-than-normal uplift (positive 500 mb vertical velocity anomalies) and is surrounded by a region of lower-than-normal subsidence (negative vertical velocity anomalies). The latitudinally contrasting anomalies of precipitation rate and 500 mb vertical velocity (and of surface wind and sea-level pressure anomalies, not shown here) reveal a northward shift in the intertropical convergence zone (ITCZ) during strong-monsoon years.
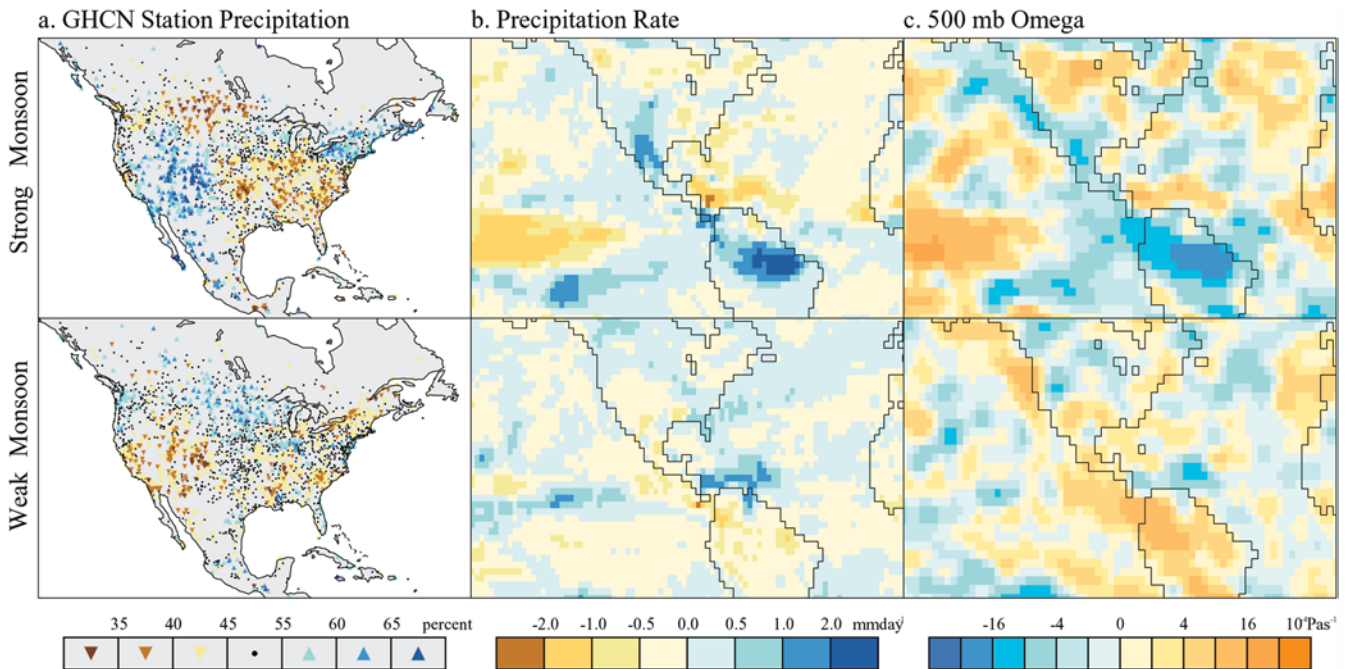
Fig. 2a–c Strong (wet)/weak (dry) monsoon composite anomalies for the present day. The composite anomalies are deviations from normal of the JJA averages for **a** station precipitation expressed as percent of normal from the GHCN data set (Peterson and Vose 1999), **b** gridded precipitation rate, and **c** 500 mb vertical velocity (omega) from the NCEP reanalysis data set (Kistler et al. 2001). The years defined by Higgins and Shi (2000) were used to define the strong (1967, 1977, 1983, 1984, 1986, 1988, 1990) and weak (1948, 1953, 1956, 1960, 1962, 1973, 1978, 1993) monsoon cases. The *colour scales* for each variable were chosen to have the same sense: *blue* indicates wetter-than-normal conditions or stronger rising/weaker sinking motions at the 500 mb level, while *orange* indicates drier-than-normal conditions or stronger sinking/weaker rising motions

Hastenrath (1985) has described a similar out-of-phase relationship between Central American precipitation and North American Great Plains precipitation. In the dust bowl years, for example, when the mid-continent of North America was dry, precipitation in Central America was greater than normal. It is possible that this multi-year out-of-phase relationship is another manifestation of the remote response shown by Higgins et al. (1997) and in our analyses. The changed orbital forcing of the mid-Holocene produces a somewhat similar pattern of precipitation anomalies (see Sect. 3), suggesting that internal dynamical processes control the spatial scale of climate response in both cases, and that at least some features of this natural mode of interannual variability are excited and amplified by the externally forced increase of summertime insolation.

3 Mid-Holocene climatology

Previous studies of the mid-Holocene in North America have shown that several kinds of palaeoenvironmental data indicate wetter-than-present conditions in the American Southwest and drier conditions elsewhere, and that some elements of this patterning can be related to the climate patterns simulated by models (Harrison 1989; Thompson et al. 1993; Webb et al. 1993; Mock and Brunelle-Daines 1999). At 6 ka, the changed orbital forcing causes increased insolation in northern summer

and autumn, and decreased insolation in northern winter and spring, thus enhancing the seasonal insolation cycle (compared to today) in the Northern Hemisphere. In the Southern Hemisphere, the amplitude of the seasonal insolation cycle is reduced. The insolation changes cause changes in temperature that are larger over land than over the ocean (because of the smaller effective heat capacity of the land surface layer) which, in turn, causes strengthening of the summer and winter monsoons in the Northern Hemisphere and weakening of the summer and winter monsoons in the Southern Hemisphere. Earlier analyses of the climate response to insolation forcing did not satisfactorily explain all features of the palaeodata. We present a new synthesis of palaeodata that updates previous studies and helps provide a motivation for a more detailed examination of the mechanisms, spatial patterns, and magnitude of monsoon changes during the mid-Holocene in the Americas.

3.1 Palaeodata sources

Palaeodata have been used to derive three independent, qualitative indicators of changes in regional water balance. Palaeoecological records provide information about changes in plant-available-moisture (PAM), i.e., the moisture available to sustain plant growth during the growing season (Farrera et al. 1999). Records of changes in lake level provide information on changes in precipitation minus evaporation (*P-E*), which over multi-an-

nual time scales is equivalent to runoff (Cheddadi et al. 1997). These estimates are in principle complementary: P-E represents the moisture lost to vegetation through runoff, so changes in the partitioning of precipitation between evapotranspiration and runoff (for example, due to changes in precipitation seasonality) would be expected to induce changes of opposite sign in PAM and P-E (Prentice et al. 1992; Farrera et al. 1999). In contrast, changes in total annual precipitation should (other things being equal) produce changes of the same sign in both indicators.

There is much evidence for an increase in aeolian activity across mid-continental North America during the mid-Holocene, including the re-activation of aeolian dunefields (see summaries in e.g., Forman et al. 1995, 2001; Dean et al. 1996), the formation of loess deposits (Feng et al. 1994; Forman et al. 2001; Muhs and Zárate 2001) and lunette dunes (Holliday 1997), and increased dust deposition into lakes (Keen and Shane 1990; Dean et al. 1996). Increased aeolian activity is primarily a reflection of a decrease in effective moisture acting through decreased vegetation cover. Thus, the evidence for increased aeolian activity during the mid-Holocene provides a third measure of changes in regional water balance and most likely reflects changes in PAM.

Our direct assessments of PAM are based on data from the BIOME 6000 project (Prentice and Webb 1998; Prentice et al. 2000). As part of this project, the vegetation patterns across North, Central and South America, today and at 6 ka, have been reconstructed from radiocarbon-dated pollen and plant-macrofossil records using an objective assignment scheme (Edwards et al. 2000; Williams et al. 2000; Thompson and Anderson 2000; Marchant et al. submitted). We have used these data to make a qualitative assessment of PAM between 6 ka and present. Following Farrera et al. (1999), these assessments were based on the observed modern distributional limits of moisture-limited biomes. There are 237 sites from North, Central and South America in the BIOME 6000 data set. Of these, 65% of the sites show no change in biome between 6 ka and 0 ka, and a further 22% of the sites show vegetation changes that are a response to changes in temperature rather than PAM. These sites are not used in subsequent analyses or for comparison with simulated regional climate changes. Three of the sites that show vegetation changes diagnostic of changes in PAM have been excluded from subsequent analyses because they are poorly dated (dating control >6 according to the COHMAP dating control scheme, indicating that the chronology was based either on a single date more than 2000 years from the 6 ka target or that it was based on bracketing dates one of which was more than 8000 years from the 6 ka target). The sites used in our analysis are listed in Table 1; an extended version of this table (listing all sites in the BIOME 6000 data base from our study region and documenting the reason for not using specific sites) is available.

Our assessments of P-E are based on geomorphic and biostratigraphic records of changes in lake level, depth or area (collectively known as lake status). Selected lake status data from North, Central and South America are presented in e.g., Markgraf et al. (2000) and Metcalfe et al. (2000). We have extracted 62 lake records from the Global Lake Status Data Base (GLSDB: Kohfeld and Harrison 2000), updated by incorporation of 20 new sites specifically coded for this study to provide a more comprehensive data set (Table 2). Eight sites are excluded from further analysis and are therefore not mapped in Fig. 3 (second panel): four because they have no sedimentary record for the 6 ka interval and four because they are poorly dated (dating control >6 according to the COHMAP dating control scheme).

We have compiled the published data documenting periods of aeolian activity during the Holocene from 181 individual radiometrically-dated sites. Reworking of aeolian deposits is commonplace and individual site records of aeolian activity are more likely to be incomplete than, for example, lacustrine records. To overcome this problem, existing syntheses of aeolian data from mid-continental North America have tended to present composite aeolian stratigraphies from individual regions (see e.g., Forman et al. 2001). However, such composite stratigraphies can be heavily influenced by individual sites which are not typical of the regional pattern. Furthermore, the compositing approach tends to obscure small-scale (intra-regional) differences in the expression and timing of aridity, which are more easily seen when the individual site data are examined. About one third of the individual records in our compilation provide no direct evidence of conditions at 6 ka because the stratigraphic records for the mid-Holocene are missing. Most of the remaining sites (79%) provide evidence for increased aeolian activity during the mid-Holocene compared to today, although at least some of the sites with quasi-continuous records through the Holocene provide information (e.g., palaeosol formation) suggesting the 6 ka was a period of relative landscape stability. Aeolian deposits are difficult to date and thus it can be difficult to determine the exact timing of periods of aridity. This problem is reflected in the large number of sites with poor dating control (47% of the 6 ka sites). Although there appears to be coherency in the spatial patterns shown by poorly dated sites and those with more reliable dating, we excluded poorly dated sites (dating control >6 according to the COHMAP dating control scheme) from our analyses; these sites are not shown on Fig. 3 (third panel). The sites used in our analysis are listed in Table 3; an extended version of this table (listing all the sites examined and documenting the reason for not using specific sites in our analyses) is available.

The reconstructions of changes in moisture-balance parameters based on data from the BIOME 6000 data set and from the GLSDB are for the interval 6 ± 0.5 ka on the radiocarbon time-scale. Although most of the aeolian records were dated using radiocarbon, some individual site chronologies were based on luminescence dating and hence expressed in calendar years. In order to ensure compatibility between the various data sets, we

Table 1 Sites providing estimates of changes in plant-available-moisture (Δ PAM), based on pollen or plant macrofossil data. The sites are arranged in alphabetical order by country. The latitude and longitude are given in degrees, where north and east are conventionally positive and south and west are negative. The dating control (DC) is given using the COHMAP scheme, as described in Yu and Harrison (1995). The number of radiocarbon or other kinds of dates used to assess the dating control is given. In the case of packrat middens, this is the date of the individual sample (which is given in brackets). The DC of some sites (marked[a]) has been recalculated, because of discrepancies between published estimates. An extended version of this table, which lists all the BIOME6000 sites in our study region (including those not used in our analyses because they are not diagnostic or poorly dated), and documents the original sources of information about each site, is available

| Name	Country	Latitude (°)	Longitude (°)	Elevation (m)	Type of data	Number of ^{14}C dates	DC 6 k	Biome 0 ka	Biome 6 ka	ΔPAM
Amarete	Bolivia	−15.23	−68.98	4000	Pollen	2	n/a	Desert	Cool grassland/shrub	Wetter
Chacaltaya 1	Bolivia	−16.36	−68.13	4750	Pollen	1	n/a	Cool grassland/shrub	Warm temperate rain forest	Wetter
Cotapampa	Bolivia	−15.21	−69.11	4450	Pollen	5	n/a	Cool grassland/shrub	Warm temperate rain forest	Wetter
Clearwater Lake[a]	Canada	50.87	−107.93	686	Pollen	2 + 1 strat.	4C	Open conifer woodland	Steppe	Drier
Riding Mountain/E Lake	Canada	50.72	−99.65	724	Pollen	8	1C	Taiga	Steppe	Drier
La Guitarra	Columbia	4.00	−74.28	3450	Pollen	3	n/a	Cool grassland/shrub	Broad-leaved evergreen/warm mixed forest	Wetter
Laguna Herrera	Columbia	5.00	−73.96	n/a	Pollen	3	n/a	Semi-arid woodland scrub	Broad-leaved evergreen/warm mixed forest	Wetter
San Jose Chulchaca	Mexico	20.86	−90.13	3	Pollen	8	2C	Xerophytic woods/scrub	Tropical dry forest	Wetter
Laguna Pomacocha	Peru	−11.75	−75.50	4450	Pollen	2	2C	Desert	Warm temperate rain forest	Wetter
Balsam Meadows	USA	37.17	−119.50	2005	Pollen	6	2C	Cool conifer forest	Open conifer woodland	Drier
Bog D	USA	47.18	−95.17	457	Pollen	4	3C	Cool mixed forest	Steppe	Drier
Cottonwood Pass Pond	USA	38.83	−106.41	3700	Pollen	3	2C	Open conifer woodland	Cool conifer forest	Wetter
Diamond Pond	USA	43.25	−118.33	1265	Pollen	11	n/a	Steppe	Open conifer woodland	Wetter
Dome Creek Meadow	USA	40.02	−107.03	3165	Pollen	5	2C	Open conifer woodland	Steppe	Drier
Emerald Lake	USA	44.07	−110.30	2634	Pollen	3	4C	Open conifer woodland	Taiga	Wetter
Gray's Lake	USA	43.00	−111.58	1946	Pollen	15	2C	Open conifer woodland	Steppe	Drier
Guardipee Lake	USA	48.55	−112.72	1233	Pollen	3	5C	Open conifer woodland	Steppe	Drier
Hay Lake, Arizona	USA	34.00	−109.43	2780	Pollen	6	6C	Steppe	Open conifer woodland	Wetter
Hurricane Basin	USA	37.97	−107.55	3650	Pollen	6	2C	Steppe	Taiga	Wetter
Ice Slough	USA	42.48	−107.90	1950	Pollen	4	3C	Open conifer woodland	Steppe	Drier
La Poudre Pass Bog	USA	40.48	−105.78	3103	Pollen	3	2C	Steppe	Open conifer woodland	Wetter
Nichols Meadow	USA	37.43	−119.57	1509	Pollen	2	1D	Cool conifer forest	Open conifer woodland	Drier
Posy Lake	USA	37.95	−111.70	2653	Pollen	4	1C	Cool conifer forest	Open conifer woodland	Drier
Swan Lake	USA	42.33	−112.42	1452	Pollen	3	4C	Open conifer woodland	Steppe	Drier
Tioga Pass Pond	USA	37.92	−119.27	3018	Pollen	4	1C	Steppe	Open conifer woodland	Wetter
Volo Bog	USA	42.35	−88.18	229	Pollen	6	1C	Steppe	Broad-leaved evergreen/warm	Wetter
White Pond	USA	34.17	−80.78	90	Pollen	3 + 2 strat.	4C	Steppe	Broad-leaved evergreen/warm mixed forest	Wetter
Wide Rock Butte	USA	36.12	−109.33	2100	Midden	n/a (6210)	1D	Open conifer woodland	Cool mixed forest	Wetter

Table 2 Sites providing estimates of changes in mean annual P-E, based on lake status data. Most of the sites are derived from the Global Lake Status Data Base (see Kohfeld and Harrison 2000); sites marked[a] were compiled for this study using the same methodology. The sites are arranged in alphabetical order by country. The latitude and longitude are given in degrees, where north and east are conventionally positive and south and west are negative. The dating control (DC) is given using the COHMAP scheme, as described in Yu and Harrison (1995). An extended version of this table, which documents the original sources of information about each site, is available

Name	Country	Latitude (°)	Longitude (°)	Elevation (m)	Number of ^{14}C dates	DC 6 ka	Coding 0 ka	Coding 6 ka	ΔP-E
Laguna Bella Vista[a]	Bolivia	-13.62	-61.55	n/a	15 (1 not used)	2C	High	Intermediate	Drier
Laguna Chaplin[a]	Bolivia	-14.47	-61.07	n/a	14 (2 not used)	1C	High	Intermediate	Drier
Tauca	Bolivia	-19.50	-68.00	3660	8 (1 not used)	7	Low	Low	No change
Titicaca	Bolivia/Peru	-16.13	-69.25	3810	7 + top	2C	High	Intermediate	Drier
Lagoa Santa[a]	Brazil	-19.63	-43.90	740	3	1D	High	Low	Drier
Lake Pata[a]	Brazil	-0.50	-67.00	300	16	1C	High	High	No change
Fiddler's	Canada	56.25	-120.75	630	3 + top	1C	High	Low	Drier
Isle	Canada	52.62	-114.43	700	3 + top + tephra	1C	High	Low	Drier
Moore	Canada	53.00	-110.50	500	6 + top	2C	High	Low	Drier
Phair Lake	Canada	50.57	-122.05	716	4 (1 not used) + top + tephra	1C	High	Low	Drier
Smallboy	Canada	53.58	-114.13	762	5 + top + tephra	1C	High	Low	Drier
Wabamun	Canada	53.54	-114.42	732	21 + top + tephra	2C	Intermediate	Low	Drier
Wedge	Canada	50.87	-115.17	1500	2 + top + tephra	2C	High	High	No change
Whitney's Gulch	Canada	51.52	-57.30	98	6 (1 not used) + top	2C	High	Low	Drier
El Abra	Columbia	5.00	-74.00	2570	8 + top	5C	Low	Low	No change
El Gobernador	Columbia	3.85	-74.35	3815	2 + top	2C	Low	Intermediate	Wetter
Fuquene	Columbia	5.50	-73.75	2580	3	7	High	High	No change
La Guitarra	Columbia	3.87	-74.00	3450	3 + top	6C	Low	Intermediate	Wetter
Parque Vicente Lachner[a]	Costa Rica	9.72	-83.93	2400	3	4C	High	High	No change
El Junco	Equador	-0.87	-89.45	650	8 + top	2C	High	Intermediate	Drier
Quexil	Guatemala	16.93	-90.12	110	7 (1 not used) + top	3C	High	High	No change
Lake Miragoane[a]	Haiti	18.40	-70.08	20	11+1210Pb	1C	Low	High	Wetter
Wallywash Great Pond	Jamaica	17.95	-77.80	7	11 (5 not used) + top	1C	High	High	No change
Babicora[a]	Mexico	29.00	-108.00	2200	12 (7 not used)	3C	Moderately high	Very low	Drier
Chichancanab	Mexico	19.50	-88.75	38	4 + top	2C	Low	Low	No change
La Piscina de Yuriria[a]	Mexico	20.22	-101.13	1740	8 (1 not used)	2C	High	Very high	Wetter
Laguna Pompal[a]	Mexico	18.25	-94.95	700	7	7	High	No record	No record
Lake Cobá[a]	Mexico	20.60	-87.75	10	8 (2 not used)	n/a	Intermediate	Low	Drier
Mexico	Mexico	19.50	-99.00	2240	26 (3 not used) + top	1C	Intermediate	High	Wetter
Patzcuaro	Mexico	19.58	-101.58	2044	9 + top	1D	Intermediate	Intermediate	No change
Punta Laguna[a]	Mexico	20.63	-87.62	14	9 (4 not used)	3C	Intermediate	No record	No record
San José Chulchaca[a]	Mexico	20.95	-90.19	3	8	n/a	High	High	Wetter
Sayauci[a]	Mexico	20.72	-80.83	> 25	5	n/a	Low	No record	No record
Upper Lerma (Chiconahuapan)[a]	Mexico	19.13	-99.52	2575	11 (1 not used)	1C	Very low	High	Wetter
El Valle[a]	Panama	-8.45	-81.20	500	8 (4 not used)	n/a	No record	No record	No record
Lake La Yeguada[a]	Panama	8.23	-84.78	600	11 (4 not used)	4C	Low	Low	No change
Laguna Jeronimo[a]	Peru	-11.78	-75.22	4450	4 (1 not used)	4C	High	High	No change
Laguna Tuctua[a]	Peru	-11.67	-75.00	4250	4	1D	High	High	No change
Lake Aricota[a]	Peru	-17.37	-70.88	2800	29 (7 not used)	1C	Low	Low	Wetter
Lake Junin[a]	Peru	-11.00	-76.17	4100	11	1D	High	High	Drier
Adobe	USA	37.91	-118.60	1951	7 + top	4D	Low	Low	No change
Annie	USA	27.30	-81.40	36	9 (2 not used) + top	4C	High	Intermediate	Drier
Bonneville	USA	40.50	-113.00	1280	211 (16 not used) + top + tephra	1D	Low	Low	No change

Table 2 Continued

Name	Country	Latitude (°)	Longitude (°)	Elevation (m)	Number of ^{14}C dates	DC 6 ka	Coding 0 ka	Coding 6 ka	$\Delta P\text{-}E$
Cahaba Pond	USA	33.50	-86.53	210	13 + top	1D	Intermediate	Low	Drier
Carp	USA	45.92	-122.88	714	13 (1 not used) + top + tephra	1D	High	Intermediate	Drier
Chewaucan	USA	42.67	-120.50	1296	6 (2 not used) + top + tephra	6D	Low	Low	No change
Cleveland	USA	42.50	-114.50	2519	4 + top + tephra	2C	High	High	No change
Clovis	USA	34.25	-103.33	1250	18 (3 not used) + top	2C	Low	Low	No change
Cochise	USA	32.13	-109.85	1260	35 (5 not used) + top	4D	Low	Low	No change
Deep Spring	USA	37.28	-118.03	1499	10 + top	3C	Low	Low	No change
Devil's Lake	USA	48.02	-98.95	430	7 + top	1C	Intermediate	Low	Drier
Diamond Pond	USA	43.09	-118.78	1341	15 (2 not used) + top + tephra	3D	Intermediate	Low	Drier
Duck Pond	USA	41.93	-70.00	3	9 + top	2C	Intermediate	Low	Drier
Elk	USA	47.21	-95.21	453	0 + varve chronology	1C	High	Low	Drier
Fort Rock	USA	43.17	-120.75	1311	14 (1 not used) + tephra	5D	Low	Low	No change
George	USA	43.52	-73.65	96	2 + top	2C	High	Intermediate	Drier
Goshen	USA	31.72	-86.13	105	8 (3 infinite) + top	2D	Intermediate	High	Wetter
Hay	USA	34.00	-109.50	2780	5 + top	4C	High	High	No change
Hook Lake Bog	USA	42.95	-89.33	260	11 + top	1C	Intermediate	Low	Drier
Jacob	USA	34.42	-110.83	2285	3 + top	7	Intermediate	Low	Drier
Kettle Hole	USA	43.00	-95.00	350	4 + top	2C	Low	Intermediate	Wetter
Kirchner Marsh	USA	44.83	-92.77	275	12 (2 not used) + top	1C	Intermediate	Low	Drier
Lahontan	USA	40.00	-119.50	1054	289 (9 not used)+Z(−41)S + tephra	3D	Low	Low	No change
Leconte	USA	33.33	-116.00	−71	63 (10 not used)	2D	Low	Low	No change
Little Salt Spring	USA	27.00	-82.17	5	18 + top	1C	High	Intermediate	Drier
Lubbock	USA	33.63	-101.90	975	113 (9 not used)	1D	Intermediate	High	Wetter
Mendota	USA	43.10	-89.42	259	24 + top	1C	Intermediate	Low	Drier
Mission Cross Bog	USA	41.75	-115.50	2424	0 + correlation	1C	High	High	No change
Okoboji	USA	43.33	-95.20	425	14 (1 not used) + top	1C	High	Low	Drier
Pickerel	USA	43.50	-97.33	395	6 + top	2C	High	Low	Drier
Ruby Marshes	USA	40.58	-115.33	1818	14 + top + tephra	1C	Intermediate	Low	Drier
Russell	USA	38.05	-118.77	1951	4 + top + tephra	7	Low	Low	No change
Rutz	USA	44.87	-93.87	314	8 + top	1D	Intermediate	Low	Drier
San Agustin	USA	33.83	-108.17	1842	20 + top	4C	Low	Intermediate	Wetter
Searles	USA	35.60	-117.70	493	110 (22 not used)	3D	Low	Low	No change
Swan	USA	41.72	-102.50	1300	2 + top	3C	High	Intermediate	Drier
Walker	USA	35.50	-111.67	2700	16	1D	Intermediate	Low	Drier
Washburn Bog	USA	43.53	-89.65	248	6 + top	1D	Intermediate	Low	Drier
Weber	USA	47.47	-91.65	559	4 + top	5C	High	Low	Drier
White Pond	USA	34.16	-80.76	90	3 + top	4C	Intermediate	Low	Drier
Wintergreen	USA	42.40	-85.38	271	10	2C	Intermediate	Intermediate	No change
Valencia	Venezuela	10.10	-67.75	402	31 (3 not used) + top	1C	High	High	No change

Fig. 3 Anomalies (6 ka minus present) of **a** plant-available-moisture (PAM) based on pollen or plant macrofossil data, **b** precipitation minus evaporation (P-E) based on lake status data, and **c** aridity based on aeolian data. PAM is defined as the moisture available to sustain plant growth during the growing season, and thus in regions where plant growth is limited by extreme (cold) temperatures will represent moisture-balance conditions during part of the year only. In contrast, P-E is a measure of mean annual changes in the water budget. The aridity index based on aeolian activity could reflect changes in regional water balance during any part of the year but because vegetation cover is an important control on deflation is most likely to reflect moisture changes during the growing season. Poorly dated sites (DC = 7) have been excluded from our analyses and so are not plotted on these maps. The changes in effective moisture shown by all three data sources are composited in **d** to facilitate comparisons with the model simulations
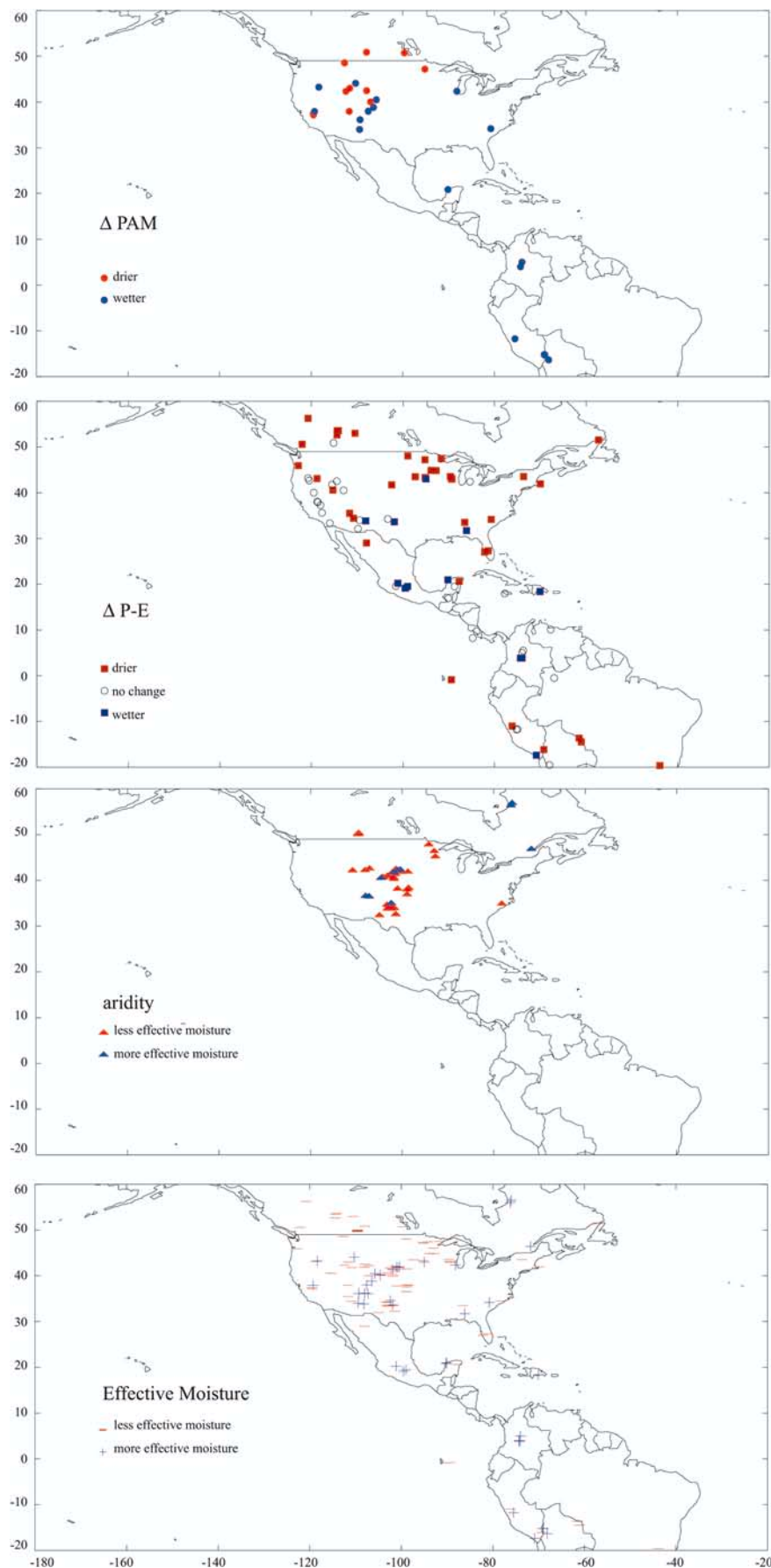
have recalculated the age models for these sites using the CALIB programme (Stuiver and Reimer 1993) to convert calendar ages to radiocarbon ages. The errors introduced by this conversion procedure are small and not likely to have a significant impact on the identification of 6 ka in the aeolian records.

The different types of palaeodata (Fig. 3) show a mutually consistent pattern of regional climate changes in northern and Central America during the mid-Holocene. Given that both the vegetation changes and the changes in aeolian activity reflect changes during the growing season (summer half year) while the lake records provide a measure of mean annual changes in moisture balance, this congruency suggests that changes in summer precipitation regimes probably dominated the annual signal of climate change in northern and Central America in the mid-Holocene. The records from the Southern Hemisphere tropics of South America do not show a mutually consistent record of regional climate changes: the vegetation data suggest conditions were wetter during the growing season but the lake data indicate drier conditions in the annual average. Given our focus on the Northern Hemisphere monsoons in this paper, we present a composite map (Fig. 3, bottom panel) showing the change in "effective moisture" by combining the data from adequately dated sites regardless of the data source. This map draws attention to the major patterns of regional climate change and thus facilitates comparison of the observations with regional climate changes simulated by FOAM and CSM.

3.2 Regional climates at 6 ka as shown by palaeodata

The different types of palaeodata (Fig. 3, bottom panel) show that conditions were wetter than present in the southeastern part of the Great Basin and extending southwards into Mexico. Wetter conditions than today were also registered in northwestern South America. In contrast, conditions drier than today extended in a crescent starting in the Pacific Northwest, through the interior plans of southern Canada and through into the central plains of North America. Most of the sites from eastern North America register temperature changes rather than changes in moisture regimes. It is thus difficult to determine the eastern limit of the arid crescent. A cluster of sites to the east of the Great Lakes register wetter conditions, as does a single site near the Gulf of Mexico. Other than these regions, the limited amount of data from eastern North America suggests moisture conditions there were similar to today (or possibly slightly drier) during the mid-Holocene. The pattern of drier-than-present conditions in the regions peripheral to the enhanced monsoon core region of the southeastern Great Basin is similar to the contemporary patterns of variability seen in the precipitation composites associated with extreme high (wet) versus extreme low (dry) states of the Arizona monsoon (see Fig. 2).

The reconstructed pattern of regional climate changes at 6 ka is not fundamentally different from that shown in previous syntheses (see e.g., Ritchie and Harrison 1993; Thompson et al. 1993; Webb et al. 1993; Dean et al. 1996; Mock and Brunelle-Daines 1999; Gajewski et al. 2000; Markgraf et al. 2000; Metcalfe et al. 2000; Muhs and Zárate 2001; Forman et al. 2001). However, by assembling data on a continental scale and combining multiple data sets, we are able to show that the regional climate changes have been coherent at a broad, continental scale (Fig. 3d). This synthesis makes apparent the clear spatial pattern with wetter-than-present conditions in Central America and the southwestern United States and generally drier-than-present conditions in the surrounding regions, a pattern that resembles the pattern prevailing during strong-monsoon years at present. This relationship strongly suggests that the changes are mechanistically linked and underscores the need to re-examine climate model simulations (Sect. 5) with the aim of developing a more comprehensive understanding of the causes of the regional wet/dry pattern evident in both recent observations and palaeodata from North America. Fewer data are available from Mexico, Central America and South America. However, the data that are available appear to indicate linkages between regional changes in Mexico, Central America and northern South America during the mid-Holocene and the monsoonal changes observed from further north. A mechanistic understanding of the role of the monsoon in North America must therefore encompass an understanding of the interplay with the monsoon precipitation of northern South America.

4 Models and experimental design

We have examined the changes in the American monsoons in response to changes in orbital forcing during the mid-Holocene (6 ka) using two dynamical atmosphere–ocean models: the Fast Ocean Atmosphere Model (FOAM: Jacob 1997) and a version of the NCAR CSM (Otto-Bliesner 1999).

The FOAM model is a fully parallel coupled ocean–atmosphere model (Jacob 1997). The AGCM component is a version of the NCAR CCM2, in which the atmospheric physics has been replaced by those of CCM3. The AGCM has been run at a horizontal resolution of R15 and 18 levels in the vertical. The OGCM is developed from the GFDL MOM ocean and has a resolution of 1.2° in latitude, 2.4° in longitude, and 16 layers in the vertical. The land surface scheme uses a simple bucket model and prescribed vegetation characteristics. FOAM has been integrated for 600 years without flux corrections and shows no climate drift. FOAM captures most major features of the observed tropical climatology and produces realistic simulations of the modern monsoons (Jacob 1997; Liu et al. unpublished). The tropical Indo-Pacific region is realistically characterized by a warm pool in the western Pacific/eastern Indian Oceans and a cold tongue in the eastern Pacific. In boreal summer, the precipitation belt associated with the ITCZ lies north of the equator over the oceans. Substantial precipitation penetrates deep into the Asian and North America continents (although part of the summer precipitation in mid-latitude North America and eastern Asia is caused by extratropical cyclones). A strong monsoon low develops over southern and eastern Asia, accompanied by high pressure over Tibet in the upper atmosphere. The surface Asian Low extends westward across northern Africa at

Table 3 Summary of geomorphic and geological evidence for changes in aridity during the Holocene. The latitude and longitude are given in degrees, where north and east are conventionally positive and south and west are negative. For those sites marked[a], the latitude and longitude is for the center of the region. The dating control (DC) is given using the COHMAP scheme, as described in Yu and Harrison (1995). An extended version of this table (listing all the sites examined and documenting the reason for not using specific sites in our analyses), and documents the original sources of information about each site, is available

Name	State/ Province	Latitude (°)	Longitude (°)	Elevation (m)	Type of site	Evidence	Timing of aridity (^{14}C ka)	Number of ^{14}C dates	Number of Other Dates	DC 6 ka	Δ aridity at 6 ka
Hardin Hairpin Dune, Fort Morgan Dune Field	Colorado	40.28	−104.45	n/a	Dune field	Parabolic dune	ca 7	0	1 (OSL)	2D	Drier
Kersey Road site, Hudson Dune Field	Colorado	40.12	−104.60	1495	Dune field	Aeolian deposits overlying soil	ca 13,500; >9.5; 5–4.8; 4–1; <0.9	7	3 (TL)	1C	Wetter
Milliron Draw, Fort Morgan Dune Field	Colorado	40.30	−104.12	n/a	Dune field	Aeolian deposits overlying soils	<5.6; <1.4	2	0	2D	Drier
Sterling Locality, Fort Morgan Dune Field	Colorado	40.63	−103.17	n/a	Dune field	Aeolian deposits overlying soils	9–3	2	0	2C	Drier
Unnamed sites, Hudson Dune Field[a]	Colorado	40.10	−104.68	n/a	Dune field	Aeolian deposits overlying soil	<7.3 ka to > 5 or 3	2	2 (TL); end established soil morphology	5D	Drier
Cullison Quarry, Great Bend Sand Prairie	Kansas	37.61	−98.88	n/a	Dune field	Palaeosols in dune sand	<7.8–>3.8	2	0	6D	Drier
Mills	Kansas	39.90	−101.80	n/a	Valley in loess	Loess deposition	<7.9	2	0	6D	Drier
Multiple sites near Garden City[a]	Kansas	37.80	−101.00	n/a	surficial loess	palaeosol underlying loess	ca 6	4	0	1D	Drier
Stafford 2, Great Bend Sand Prairie	Kansas	37.96	−98.63	n/a	Dune field	Palaeosols in dune sand	ca 10.4–1; <1	2	0	5C	Drier
Stafford 3, Great Bend Sand Prairie	Kansas	37.89	−98.60	n/a	Dune field	Palaeosols in dune sand	>6.1; <6.1–1	1	0	1D	Drier
Elk Lake	Minnesota	44.83	−92.77	275	Lake	Thickness of clastic varves	7.1–3.8	0	varve chronology	1C	Drier
Lake Ann	Minnesota	46.00	−93.00	n/a	Lake	Magnetic susceptibility record of aeolian influx	8–4; maxima at 7.4, 5.8 and 4.9	2	0	1C	Drier
Lake Winnibigoshish	Minnesota	47.45	−94.20	n/a	Fossil dunes	Dunes with palaeosols	8–4	2	0	1C	Drier
Bignell Hill	Nebraska	41.00	−101.50	n/a	Loess mantled bluff	Loess deposition	ca 10–1.4	6	2	5C	Drier
Blue Creek Valley, Nebraska Sand Hills	Nebraska	41.50	−102.00	1135	Lakes in blocked valley	Dune damming	12–10.5; ca 6–4; <1.5	14	0	1D	Drier
Collier, Nebraska Sand Hills	Nebraska	41.78	−100.40	n/a	Dune field	Sand overlying organic deposits	<7	1	0	5D	Drier
Devils Den	Nebraska	41.46	−100.19	n/a	Loess mantled bluff	Loess deposition	9–3	2	7 (TL)	2C	Drier
Dismal River Ranch (B), Nebraska Sand Hills	Nebraska	41.85	−101.00	n/a	Dune field	Peat overlain by dune sand	<5	2	1TL	2C	Wetter
Hoover Blowout	Nebraska	40.25	−101.90	n/a	Dune field	Aeolian deposits overlying soils	>7.9; <7.8	2	0	6D	Drier
Mirdan Canal Section, Loupe River Basin	Nebraska	41.50	−98.75	ca 2150	Loess plateau	Palaeosols in loess	ca 9, 8.7–>3	4	0	3C	Drier

Table 3 Continued

Name	State/Province	Latitude (°)	Longitude (°)	Elevation (m)	Type of site	Evidence	Timing of aridity (^{14}C ka)	Number of ^{14}C dates	Number of Other Dates	DC 6 ka	Δ aridity at 6 ka
Natick, Nebraska Sand Hills	Nebraska	41.95	−100.43	n/a	Dunes	Dunes overlying paludal deposits	<2.6	3	0	4D	Wetter
Whitetail Creek, Nebraska Sand Hills	Nebraska	41.37	−101.87	n/a	Dune field	Dunes overlying paludal deposits	>9.9; <2.9	5 (2 dup. fractions)	0	3C	Wetter
Whitman Site, Middle Loup River	Nebraska	42.08	−101.38	1060	River bank	Fossil dune	<8–3; 1.8–0.3	6	3 (OSL)	2C	Drier
Bluitt Cemetery	New Mexico	33.45	−103.15	n/a	Lunette	Aeolian sands in lunette	<7.8, 8–4.5	2	0	6D	Drier
Clovis, Muleshoe Dunes	New Mexico	34.27	−103.33	n/a	Dune field	Aeolian deposits	>4.8, <4.8–>1	11 (3 not used)	Archaeologic	5D	Drier
Escavada Wash, Chaco Dune Field	New Mexico	36.10	−107.25	n/a	Dune field	Aeolian deposits overlying soils	4–<2.2	5	0	n/a	Wetter
Tsaya Wash, Chaco Dune Field	New Mexico	36.20	−108.00	n/a	Dune field	Aeolian deposits overlying soils	5.6–<2.8	2	0	2D	Wetter
Cape Fear River[a]	North Carolina	34.50	−78.25	n/a	Fossil dunes	Dune formation on fluvial terraces	7.7–5.7 to 3.5	9 (5 infinite)	0	1D	Drier
Cimarron River Dune Field[a]	Oklahoma	36.53	−98.93	n/a	Dunes on river terraces	Palaeosols in dunes	11–8, 7.5–6.5, <6.3, <1.2	4	0	2D	Drier
Eastern shore, Hudson Bay[a]	Quebec	56.00	−76.25	n/a	Dune field	active dunes overlying soil	<5	101	0	4D	Wetter
Eastern shore, Hudson Bay[a]	Quebec	56.50	−76.00	n/a	Dune field	Palaeosols in dunes	<6; maxima ca 1.2 and 0.5	196	0	1D	Wetter
St. Flavian site, St. Lawrence Lowlands	Quebec	46.45	−71.78	130	Dune field	Paludification of dune field	10–7.5	21	0	2C	Wetter
Dean's Site	Saskatchewan	49.96	−109.50	760	Reservoir bluff	Loess deposition	Mid-Holocene	0	Mazama tephra	3D	Drier
Downie Lake Site	Saskatchewan	49.80	−109.68	884	Lake bluff	Loess deposition	Mid-Holocene	0	Mazama tephra	3D	Drier
Eagle Camping Site	Saskatchewan	49.97	−109.52	756	Valley cliff	Loess deposition	Mid-Holocene	0	Mazama tephra	3D	Drier
Friday's Site	Saskatchewan	49.85	−109.57	823	Slump scarp	Loess deposition	<10.5 – <6.8	1	Mazama tephra	3D	Drier
Lawrence's Fan Sire	Saskatchewan	49.70	−109.55	814	Cutbank	Loess deposition	Mid-Holocene	0	Mazama tephra	3D	Drier
Reservoir-dam Channel Site	Saskatchewan	49.97	−109.52	759	Reservoir bluff	Loess deposition	Mid-Holocene	0	Mazama tephra	3D	Drier
Southward Fan Site	Saskatchewan	49.69	−109.58	828	Cutbank	Loess deposition	Mid-Holocene	0	Mazama tephra	3D	Drier
Able's Well Wash, Red Dunes, Salt Basin	Texas	31.97	−104.97	n/a	Dune field	Palaeosols in dune sands	>6.4 to 1.7	2	0	2D	Drier
Bentley West	Texas	33.40	−102.80	n/a	Lunette	Aeolian sands in lunette	<7.9, 8–5	3	0	5D	Drier
Lewis Pit, Lea-Yoakum Dunes	Texas	33.63	−103.04	n/a	Dune field	Aeolian deposits	11.5–9.5, >6.1	1	Archaeologic	1D	Drier
Lubbock Lake (Cone Playa)	Texas	33.55	−101.72	n/a	Lunette	Aeolian sands in lunette	<6.7, <6.1, 6.5–4	9	0	1D	Drier
Rabbit Road, Muleshoe Dunes	Texas	34.18	−102.77	n/a	Dune field	Aeolian deposits	11.5–9.5, <7.6	3 (2 not used)	Archaeologic	6D	Drier

Site	Region	Latitude	Longitude		Deposit	Feature	Age		Dating	Dim.	Response
Red Lake	Texas	32.20	−101.40	n/a	Aeolian deposits	Dune field	>8.5, <8.5, 1.8–1.7	9 (2 not used)	0	1D	Drier
Sheppard	Texas	34.62	−102.40	n/a	Aeolian sands in lunette	Lunette	<5.5	3	0	2D	Wetter
Terry County, Seminole Sand Sheet	Texas	33.38	−102.45	n/a	Aeolian deposits	Dune field	<7.7, >0.4	2	0	6D	Drier
Clear Creek, Ferris Dune field	Wyoming	42.20	−107.13	>2000	Dune and interdune deposits	Dune field	7.6–7, 6–4.5	9	6 (OSL)	1C	Drier
Finley Archaeological site, Killpecker Dune Field	Wyoming	41.84	−108.11	>1700	Aeolian sands overlying pond sediments	Dune field	10–5.8, <2.8	4	Archaeologic dating	1D	Drier
Shute Creek area, Opal Dune Field	Wyoming	41.78	−110.83	99	Sand wedges overlain by dune sands	Fossil dunes	Maximum: 7.5–4; at least 2 phases < 4	9 (2 not used)	Archaeologic dating	2D	Drier

about 20°N. This extension is accompanied by a high pressure ridge in the upper air and characterises the northern Africa monsoon. A surface low pressure is centered over the American Southwest and Mexico, again accompanied by a high pressure ridge in the upper atmosphere, forming the North America monsoon (Adams and Comrie 1997). The surface low pressure systems are accompanied by substantial southwesterly monsoon winds and heavy precipitation, especially in northern Africa and South Asia, but also in North and Central America. In austral summer, the precipitation belt associated with the ITCZ migrates into the Southern Hemisphere. This migration is accompanied by a reversal of surface wind directions (i.e. development of Northern Hemisphere winter monsoons), which is most marked in Asia but also clearly demonstrated in the American Southwest monsoon region. Surface low pressure centers develop over South America and southern Africa during the austral summer, accompanied by high pressure ridges in the upper atmosphere, and marking the development of the Southern Hemisphere summer monsoon systems. FOAM also successfully reproduces tropical climate variability, including the signals of the El Nino-Southern Oscillation (ENSO: Jacob 1997; Liu et al. 1999b, 2000), tropical Atlantic variability (Liu and Wu 2000) and Pacific decadal variability (Liu et al. 2002).

The CSM is a global coupled climate model, also without flux adjustments (Boville and Gent 1998). It consists of an AGCM (CCM3: Kiehl et al. 1996), an OGCM (the NCAR CSM Ocean Model, NCOM: Gent et al. 1998), a thermodynamic and dynamic sea-ice model (Weatherly et al. 1998), and a land surface biophysics model (LSM1.0: Bonan 1998). Descriptions of the model climatology and comparisons with modern observations are given in Boville and Gent (1998) and in Boville and Hurrell (1998). The version of NCAR CSM used here has a horizontal resolution of T31 for the atmosphere and land-surface components, and a variable 3-dimensional grid (25 vertical levels, 3.6° longitudinal grid spacing and a latitudinal spacing of 1.8° poleward of 30° decreasing to 0.9° within 10° of the equator) for the ocean and sea ice models (Otto-Bliesner 1999). Extensive sensitivity experiments show that the CSM-T31 reproduces virtually all the major features of the standard CSM. Compared with FOAM, the CSM-T31 has a higher atmospheric resolution and more complete model physics.

It is useful to present results from two models in order to demonstrate the robustness of the results (see e.g., Joussaume et al. 1999, which analyses the results of 18 models participating in the Palaeoclimate Modelling Intercomparison Project) and to illustrate, where possible, how different model configurations may produce differences in detail. For example, the atmospheric portion of the CSM provides greater spatial resolution than FOAM, and the CSM also has more detailed representation of the land surface processes and sea ice (Table 4). The ocean portion of FOAM has greater longitudinal resolution than CSM. The efficient parallel coding of FOAM and the lower resolution of the FOAM atmosphere make it computationally efficient to run the coupled FOAM simulations for longer than was possible with CSM. Thus, the FOAM experiments are integrated for 150 years, starting from the 450th year of an existing modern control simulation. The last 120 years of the simulation are used to construct the monthly ensemble averages. The CSM simulations are integrated for 50 years with the last 30 years being used to construct the monthly means. There are no trends, either in mean climate or variability, through the 120 years of the FOAM simulation; thus the use of a longer period for deriving averages from FOAM compared to CSM should not affect the results presented here.

We present results using the modern calendar for both the present and mid-Holocene experiments. Although use of celestial calendar months might provide a more exact representation of climate changes during the Holocene (Kutzbach and Gallimore 1988; Joussaume and Braconnot 1997), in the present case the differences resulting from using the two calendars are small and not significant. Our conclusions remain valid using both calendars.

We have calculated the statistical significance of the response of FOAM and CSM to orbital forcing, using a two-tailed t-statistic, a 95% confidence level, and variance estimates from each model's internal variability. In the discussion of the simulated changes in

Table 4 Characteristics of the FOAM and CSM models, and orbital parameters specified in the 6 ka and control experiments

	FOAM	CSM
Atmospheric resolution	R15	T31
Ocean resolution	2.4 long × 1.4 lat, 16 vertical levels	3.6 long × 1.8 lat (30–90), decreasing to 0.9 lat between 10N–10S, 25 vertical levels
Land surface	Simple bucket	LSM 1.0
Sea ice	Implicit	Thermodynamic
References	Jacob (1997), Liu et al. (2000)	Otto-Bliesner (1999)
CO_2 0 ka	330 ppmv	280 ppmv
CO_2 6 ka	330 ppmv	280 ppmv
0 ka eccentricity	0.016724	0.016724
0 ka tilt	23.446°	23.446°
0 ka angle of perihelion defined from autumn equinox	102.04°	102.04°
6 ka eccentricity	0.018682	0.018682
6 ka tilt	24.105°	24.105°
6 ka angle of perihelion defined from autumn equinox	0.87°	0.87°
Length of simulation, 0 ka	150 years	50 years
Length of simulation, 6 ka	150 years	50 years
Length of ensemble average, 0 ka	120 years	30 years
Length of ensemble average, 6 ka	120 years	30 years

temperature and precipitation, we focus on those features of the results that are statistically significant (unless specifically noted) and in particular we concentrate on changes during the summer (JJA) and winter (DJF) seasons. In the FOAM simulation, for example, the precipitation increase in the model's core-monsoon region of the American Southwest is significant for the months from April through August, with the largest increase occurring in August (Fig. 4 top). In the CSM simulation, the precipitation increase is significant for the months from July through September, with maximum increases in July and August (Fig. 4 bottom). Thus, only the JJA (and annual) average results from this region are statistically significant for both models. In a similar spirit, we confine our analyses to changes in mean climate; analyses of the frequency distribution of precipitation over key regions shows no significant difference (*F*-test, 95% confidence interval) in variance between the control and 6 ka simulations for either FOAM or CSM.

We used FOAM to make an additional simulation for 6 ka using prescribed modern sea-surface conditions instead of the fully coupled model. Comparison of the results of the experiment with prescribed modern sea-surface temperatures (SSTs) and the experiment with full atmosphere–ocean coupling isolates the effect of ocean feedbacks on the monsoon response, and allows us to compare the sign and magnitude of ocean feedback to the sign and magnitude of the more direct response of the climate over land to insolation changes (see e.g., Kutzbach and Liu 1997; Liu et al. 1999b, unpublished). The prescribed SSTs used in this experiment were derived from the FOAM control simulation. We derived daily SST values by linear interpolation between the mean monthly values over the last 120 years of the coupled simulation. The prescribed SST simulation was run for 15 years and comparisons with the fully coupled results were made using ensemble averages of the last 10 years.

5 Results

5.1 The coupled atmosphere/ocean response of the mid-Holocene Northern Hemisphere summer (JJA) monsoon to orbital forcing

In response to increased insolation in Northern Hemisphere summer and early autumn at 6 ka (Fig. 5 left), the North American continent is warmer, the adjacent subtropical and midlatitude oceans are slightly warmer, and the equatorial ocean is cooler. The change in the equatorial Pacific is due to the dynamic (upwelling) response to a stronger Walker circulation, which in turn is linked to the strengthened Asian monsoon (Liu et al. 1999b, 2000). Parts of extreme northern South America are cooler (opposite to the expected direct radiative effect) due to increased cloudiness and precipitation. A similar effect has been noted in analyses of changes in the mid-Holocene African monsoon, where cooling caused by increased cloudiness and precipitation is also associated with orbitally forced monsoon enhancement (see e.g., Broström et al. 1998).

Sea-level pressure falls over the warmer North American continent and, in association with this decrease in pressure over the land, pressure increases in the regions of the oceanic subtropical highs (STHs), especially on their northern flanks. The STHs are thereby effectively shifted slightly northwards, causing an enhancement of the modern seasonal shift. There are enhanced northerlies along the west coast of North America and enhanced trades along the southeast coast. Southerly flow develops over the northern tropical oceans as a consequence of the colder equatorial zone and the northward-displaced STHs (see e.g., Hastenrath 1990). The northward-directed flow is associated with the northward-displaced ITCZ-like convergence/precipitation band, which, in turn, contributes significantly to onshore moisture advection and to the rainfall increase over Central America. Precipitation is increased in northern South America (by 0.6 mm/day on area average: Table 5), western Central America (by 0.4 mm/day: Table 5), and parts of the American west (by 0.6 mm/day: Table 5). Although the largest increases occur in summer (with a pronounced maximum in August), precipitation increases begin in April and May in the model's
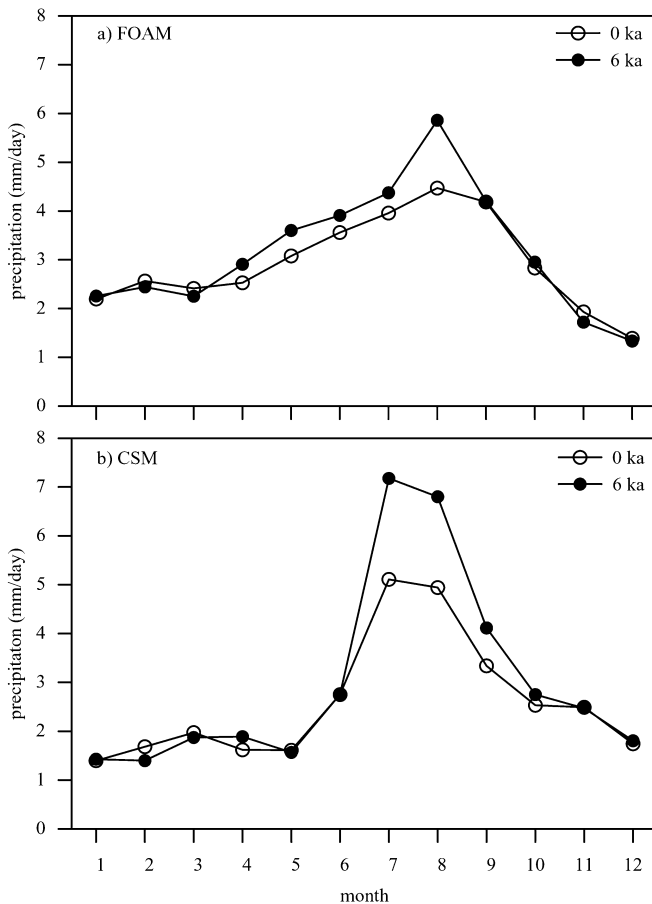
Fig. 4 The seasonal cycle of precipitation as simulated by **a** FOAM and **b** CSM in the 0 ka and 6 ka simulations over the model's core summer monsoon region in the American Southwest (approximately 25–40°N and 100–110°W). The months are conventionally numbered from 1 (January) to 12 (December). Changes in precipitation are statistically significant (*t*-test, 95% confidence level) from April through August (months 4 to 8) in the FOAM coupled OAGCM simulation, and from July through September (months 7 to 9) in the CSM coupled OAGCM simulation

core-monsoon region of the American Southwest (Fig. 4 top).

The simulated changes in pressure distribution, winds and advection in response to an enhanced seasonal insolation cycle closely resemble the patterns of both observed and simulated circulation features in the normal seasonal climatology. Hoskins (1996) and Rodwell and Hoskins (2001), using diabatic heating distributions to force a primitive equation atmospheric model, show that the heating associated with summer monsoons creates a Rossby-wave response that builds the oceanic subtropical high to the west of the monsoon region and a Kelvin-wave response that builds the equatorward portion of the subtropical high to the east of the monsoon region and thereby strengthens the trade winds that help to advect moisture into the region. These features are present in JJA (Fig. 5) in the simulations with enhanced seasonal insolation, and therefore the processes described by Hoskins (1996) and Rodwell and Hoskins

(2001) provide a dynamically based explanation for the simulated response to orbital forcing.

In addition to these first-order responses to the enhanced seasonality of insolation, the increased upward vertical motion and precipitation in Central America and the American Southwest is associated with a surrounding crescent-shaped area of increased downward vertical motion (subsidence) and decreased precipitation; this feature of the response is generally consistent with the simulations of the response to monsoonal heating shown in the study of Rodwell and Hoskins (2001). In FOAM, this feature is apparent in the Pacific Northwest, across southern Canada and the northern Great Plains, and extending south to the Gulf of Mexico. The model simulates decreased precipitation in the Pacific Northwest, southeastern North America and the Gulf Coast. Although the model simulates increased precipitation across the Great Plains, the increase is small compared to the large increase in the American Southwest.

The CSM (Fig. 5 right) has similar patterns of response in most regions. The surface temperature change is similar, except the warming in the North Pacific is somewhat larger in CSM than in FOAM, while the warming in the North Atlantic is less marked in CSM than in FOAM. The decrease in surface pressure over North America extends farther eastward in CSM than in FOAM. Both models show a similar change in pressure and winds over the North Pacific. In the North Atlantic, however, the increase in surface pressure in CSM occurs farther to the north than it does in FOAM. The changes in surface winds are therefore different in the North Atlantic sector in the two models. The inferred northward-displacement of the ITCZ occurs in CSM, as it does in FOAM, although the details of the shift are slightly different. The simulated increase of precipitation in the American Southwest follows the topographic features of that region more closely in CSM than in FOAM, because of the higher resolution of orography and atmospheric dynamics in the former model. The simulated changes in precipitation over the American Southwest occur during July through into September (Fig. 4 bottom). Thus, the monsoon season starts later and is prolonged into the autumn compared to FOAM (Fig. 4 top). This difference reflects the somewhat more pronounced differentiation in the seasonal cycle of precipitation in the CSM model. In CSM, the crescent-shaped area of subsidence and decreased precipitation is located farther south than in FOAM. FOAM simulates increased precipitation both offshore and over Central America, while CSM has a small region of decreased precipitation along the western coast of Central America that has the appearance of breaking the connection between the northward-shifted ITCZ and the increased rains over Central America (Fig. 5). It is not possible to explain this difference between the two simulations completely; it may be related to the fact the western coastal waters are slightly warmer in FOAM compared to the control, whereas this region is slightly cooler in
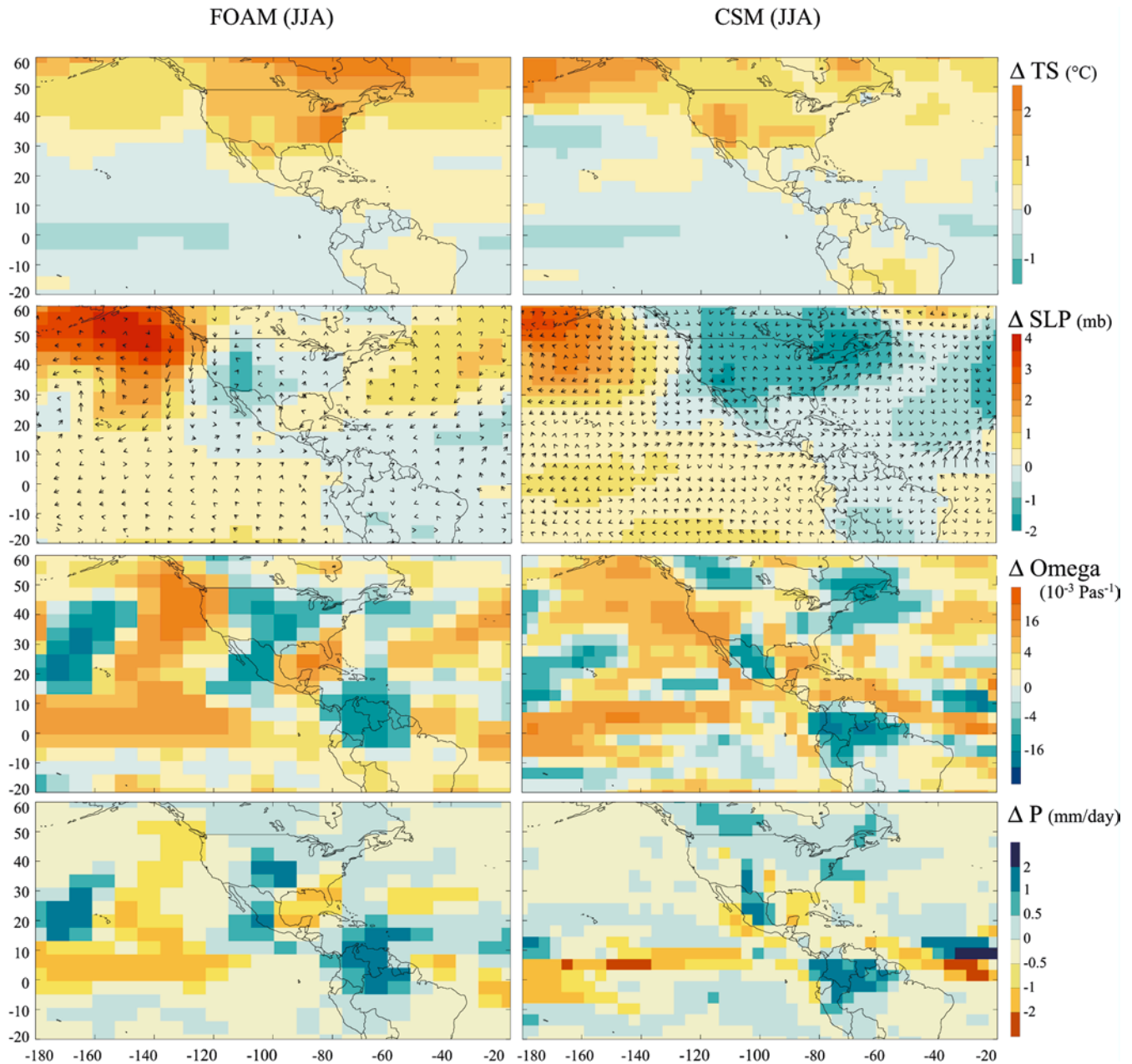
Fig. 5 Anomalies (6 ka minus 0 ka) of summer (June, July, August: JJA) surface temperature (*TS*), sea level pressure (*SLP*) and surface winds, 500 mb vertical motion (omega), and precip-itation (*P*) from the FOAM (*left*) and CSM (*right*) coupled OAGCM simulations

CSM compared to its control. Given that the two models have different physical parameterizations and different resolutions, the structure of the climatic response to orbital forcing is remarkably similar in both models.

We believe that the dynamical features described here are robust responses to orbital forcing. Not only are they shown in both the FOAM and CSM simulations, but they are also seen in simulations of the response to early Holocene (unpublished 11 ka simulation with FOAM at R15 and a dynamical ocean) and even last interglacial (Montoya et al. 1998, 2000) changes in or-bital forcing. Similar patterns have been seen in a 6 ka

experiment using the GENESIS model with a mixed-layer ocean and fully coupled dynamic vegetation (Doherty et al. 2000).

The broad features shown in the model simulations provide an explanation for the spatial patterns shown by palaeo-observations (Fig. 3). Thus, the simulated precipitation increases in the American Southwest are located in the region where the palaeodata show a shift to more moisture-demanding vegetation and an increase in lake levels. The available data from Central America and the northern part of South America also show an increase in moisture indicators, in agreement with the simulated changes in precipitation. The simulated

Table 5 Area-averaged winter (DJF), summer (JJA) and mean annual (Annual) precipitation (mm/day) for key regions at 0 ka and 6 ka as simulated in the coupled FOAM experiments, and decomposition of the total precipitation change into the amount due to direct radiative forcing (ΔR) and SST feedbacks (ΔSST). The values have been rounded and adjusted so that Δtotal = ΔR + ΔSST. Wetter is indicated by [+] and drier by [–], while wetting or drying by 10% or more is indicated by [+ +] and [– –] respectively. Consecutive months of wetter/drier conditions are listed, with the wettest/driest months underlined

Area	DJF			JJA			ANNUAL		
	0 ka	6 ka	(ΔR, ΔSST)	0 ka	6 ka	(ΔR, ΔSST)	0 ka	6 ka	(ΔR, ΔSST)
Pacific NW, N Plains, Mississippi Valley, Gulf (40–50N, 130–80W) and (30–40N, 95–80W)	2.1	2.1	(–0.1, 0.1)	4.2	4.2 [–] ASOND	(∼0, ∼0)	2.9	2.7 [–]	(–0.1, –0.1)
American West (30–40N, 120–95W)	2.7	2.7	(–0.3, 0.3)	4.0	4.6 [+ +] AMJJASO	(0.4, 0.2)	3.0	3.2 [+]	(0.1, 0.1)
Central America (12N–30N)	1.9	2.0 [+] DJFMAM	(0.4, –0.3)	5.0	5.4 [+] ASO	(–0.2, 0.6)	3.0	3.3 [+ +]	(0.1, 0.2)
N South America (0–12N)	1.4	1.3 [–]	(–0.1, ∼0)	8.8	9.4 [+] MJJASO	(0.7, –0.1)	5.5	5.6 [+]	(0.2, –0.1)
S South America (0–20S)	7.5	5.9 [– –] DJFMAM	(–1.5, –0.1)	1.3	1.6 [+ +] JASON	(0.6, –0.3)	5.3	4.9 [–]	(–0.3, –0.1)

decrease in precipitation which characterises the crescent-shaped area surrounding the monsoon core in North America coincides with the regions where the palaeodata show shifts towards less-moisture demanding vegetation, reduced lake levels or renewed aeolian activity in the Pacific Northwest, the central Great Plains and the continental interior. The palaeodata show relatively little change compared to present along the east coast of North America, again consistent with the simulations where the changes in precipitation are small and non-significant.

5.2 The role of direct radiative forcing over land on the mid-Holocene Northern Hemisphere summer (JJA) monsoon

The response to 6 ka insolation forcing in the FOAM simulations with fixed modern SSTs (Fig. 6, left) is characterised by a similar increase of surface temperature and decrease of sea-level pressure over land, and a similar compensating increase of pressure over the ocean, as in the coupled ocean–atmosphere simulation (Fig. 5). Increased low-level convergence and upward vertical motion (not shown) contribute strongly to the increase of precipitation over northern South America and parts of the American Southwest that was observed in the coupled simulation. The areally averaged increase in precipitation over northern South America is 0.7 mm/day, while the increase in the American West is 0.4 mm/day (Table 5). However, the direct response of precipitation to orbital forcing (in the absence of ocean feedbacks) in Central America is comparatively weak (positive on the west coast, negative on the east coast). Indeed, the area-averaged change in precipitation over Central America in consequence of radiative forcing alone is slightly negative (–0.2 mm/day: Table 5.).

5.3 The role of SST feedback on the mid-Holocene Northern Hemisphere summer (JJA) monsoon

The role of SST feedback can be assessed by comparing the response to orbital forcing in the fixed SST and fully-coupled FOAM 6 ka simulations. This comparison (Fig. 6) indicates that equatorial cooling and the concomitant increase in sea-level pressure, and the mid-latitude oceanic warming and concomitant weakening and enhanced northward shift of the STHs, are features that result from the coupling of atmosphere and ocean. The equatorial cooling is related to the dynamical upwelling response (Liu et al. unpublished) while the mid-latitude oceanic warming is primarily a thermodynamic response to the increased insolation, modified by the effect of changed wind speeds on evaporation (Kutzbach and Liu 1997; Liu et al. unpublished). Associated with the change in the subtropical north–south pressure gradient, southerly wind anomalies develop at 10–20°N in the Pacific, and a band of increased precipitation is found centered near 15°N associated with the northward displacement of the ITCZ. The SST feedback is associated with enhanced onshore moisture transport that significantly enhances the precipitation over Central America (by 0.6 mm/day: Table 5) while slightly enhancing precipitation over the American West (0.4 mm/day: Table 5). However, the northward shift of the equatorial precipitation band that enhances precipitation in Central America and the American West has a negative feedback effect on precipitation in northern South America (–0.3 mm/day: Table 5).

The northward and onshore flow along the western coast of Central America may also be aided by the small simulated lowering of sea-level pressure offshore. This lowering of SLP may possibly be associated with westward propagation of the enhanced surface low pressure center from land to ocean at around 25–30°N. Such a

◄
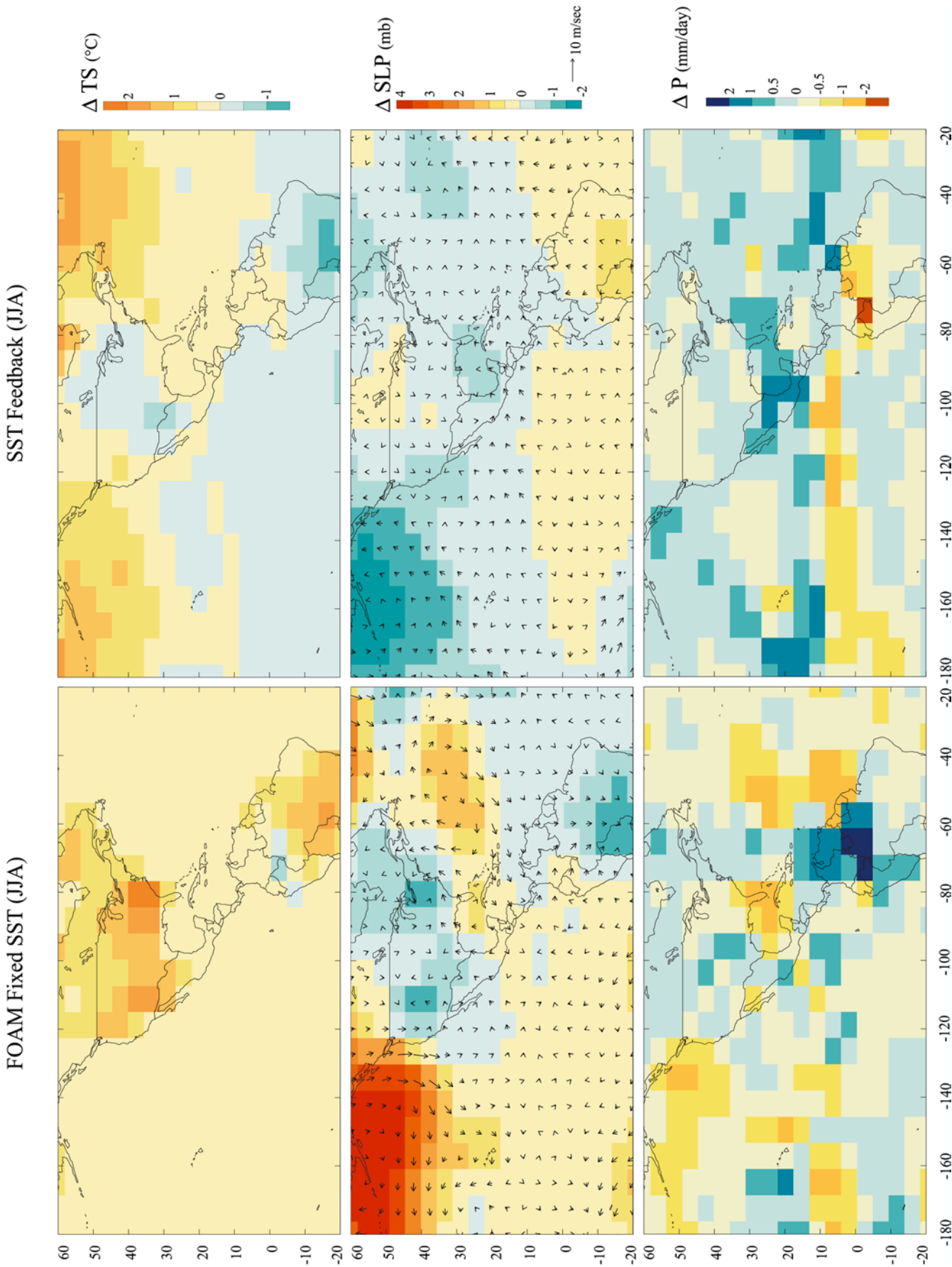
Fig. 6 Anomalies (6 ka minus 0 ka) of summer (June, July, August: JJA) surface temperature (*TS*), sea level pressure (*SLP*) and surface winds, and precipitation (*P*) from the FOAM simulation made with fixed (modern) sea-surface temperatures and reflecting the direct response to orbital forcing over land (*left*) as compared with the SST feedback response (*right*), obtained by subtracting the results with fixed SSTs from the results of the fully-coupled FOAM simulation

westward-propagation mechanism has been described by e.g., Rodwell and Hoskins (1996).

The SST feedback is crucial to the simulated increase in precipitation over Central American. The land area of Central America is not extensive enough to generate a large direct radiative response in the models. Thus, the direct radiative response over land tends to produce two separate precipitation maxima, one over northern South America and the other over parts of the American Southwest. The SST feedback, by amplifying the precipitation increase over Central America, leads to a

Fig. 7 Diagnosis of the changes in summer (June, July, August: JJA) precipitation between 6 ka and 0 ka. The *top panel* shows the change in precipitation from the fully coupled FOAM experiment, the *middle panel* shows the change in precipitation in the fixed SST FOAM simulation, and the *bottom panel* shows the difference between the two simulations (i.e. the quantitative effect of SST feedbacks)
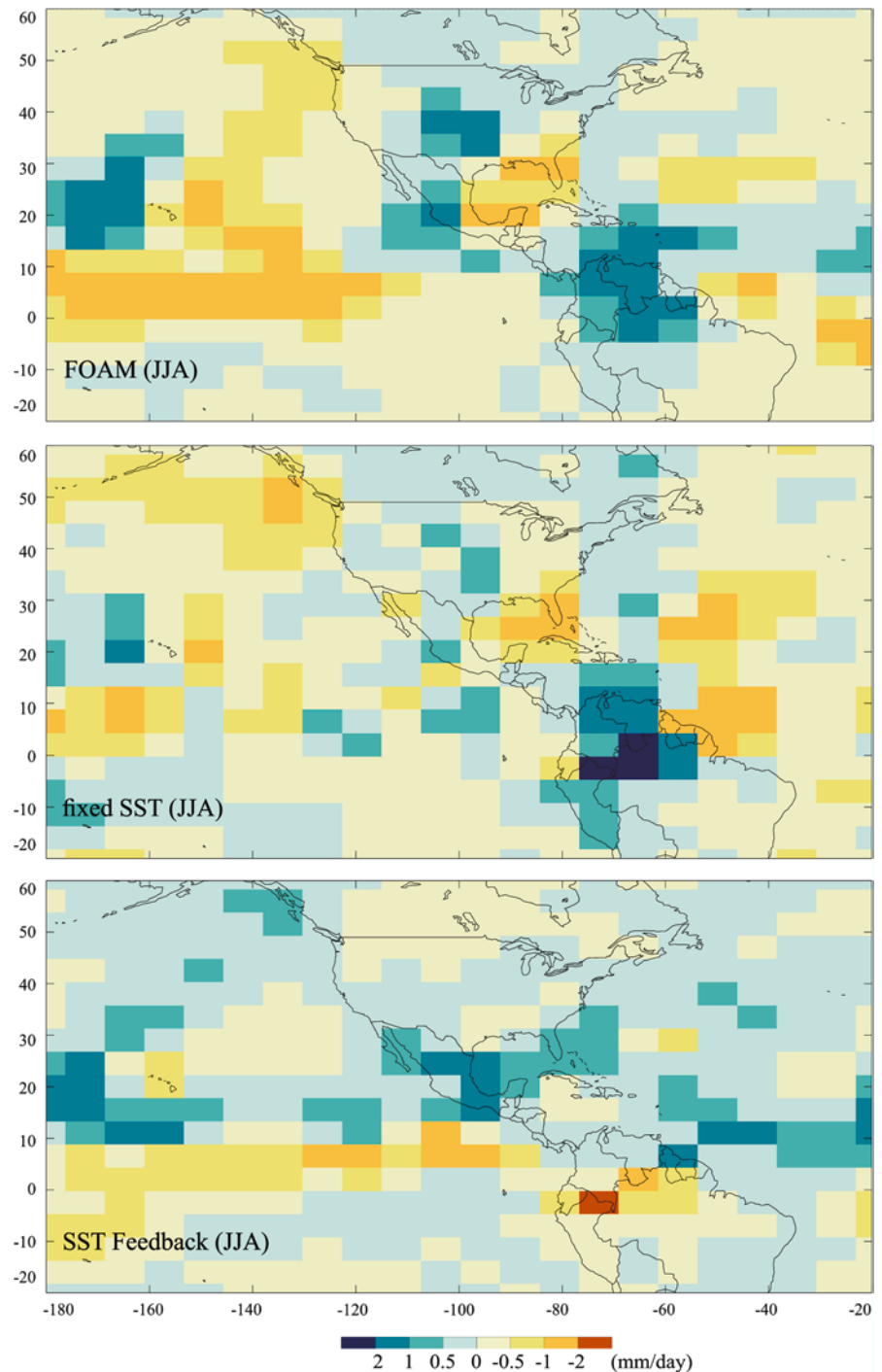
more-or-less continuous region of increased precipitation from northern South America through Central America and into the American Southwest (Fig. 7).

5.4 The coupled atmosphere/ocean response of the mid-Holocene Northern Hemisphere winter (DJF) monsoon to orbital forcing

In response to the decreased insolation in DJF, FOAM simulates a small cooling of the American Southwest, Central America, and northern South America (Fig. 8 left). There is substantial warming at high latitudes. This feature is related to sea-ice/temperature feedbacks from the enhanced insolation of the previous autumn (e.g., Kutzbach and Gallimore 1988; Mitchell et al. 1988) and is opposite to the expected direct response to DJF orbital forcing; this is possible because high-latitude DJF insolation is low under all orbital configurations. Sea-level pressure is increased slightly over the central part of the continent. Pressure is lowered over the Pacific (enhanced Aleutian low). The mid-troposphere westerlies are somewhat stronger across the Pacific at 30°N and across Central America at 15°N. Precipitation is decreased over most of northern North America (not statistically significant), but increased along the west coast and across Central America and the Gulf Coast. The mixing of these two signals means that the areally av-
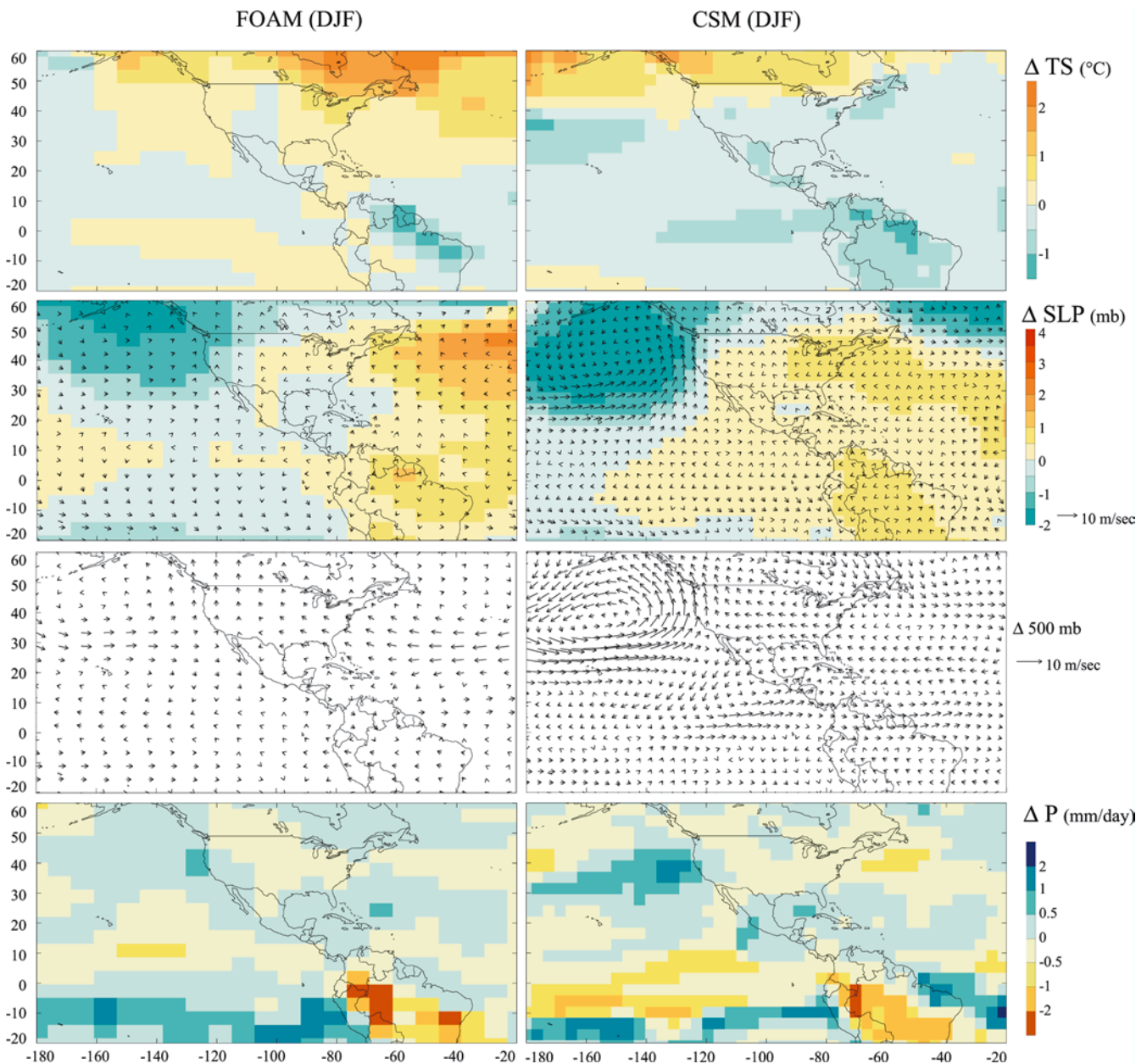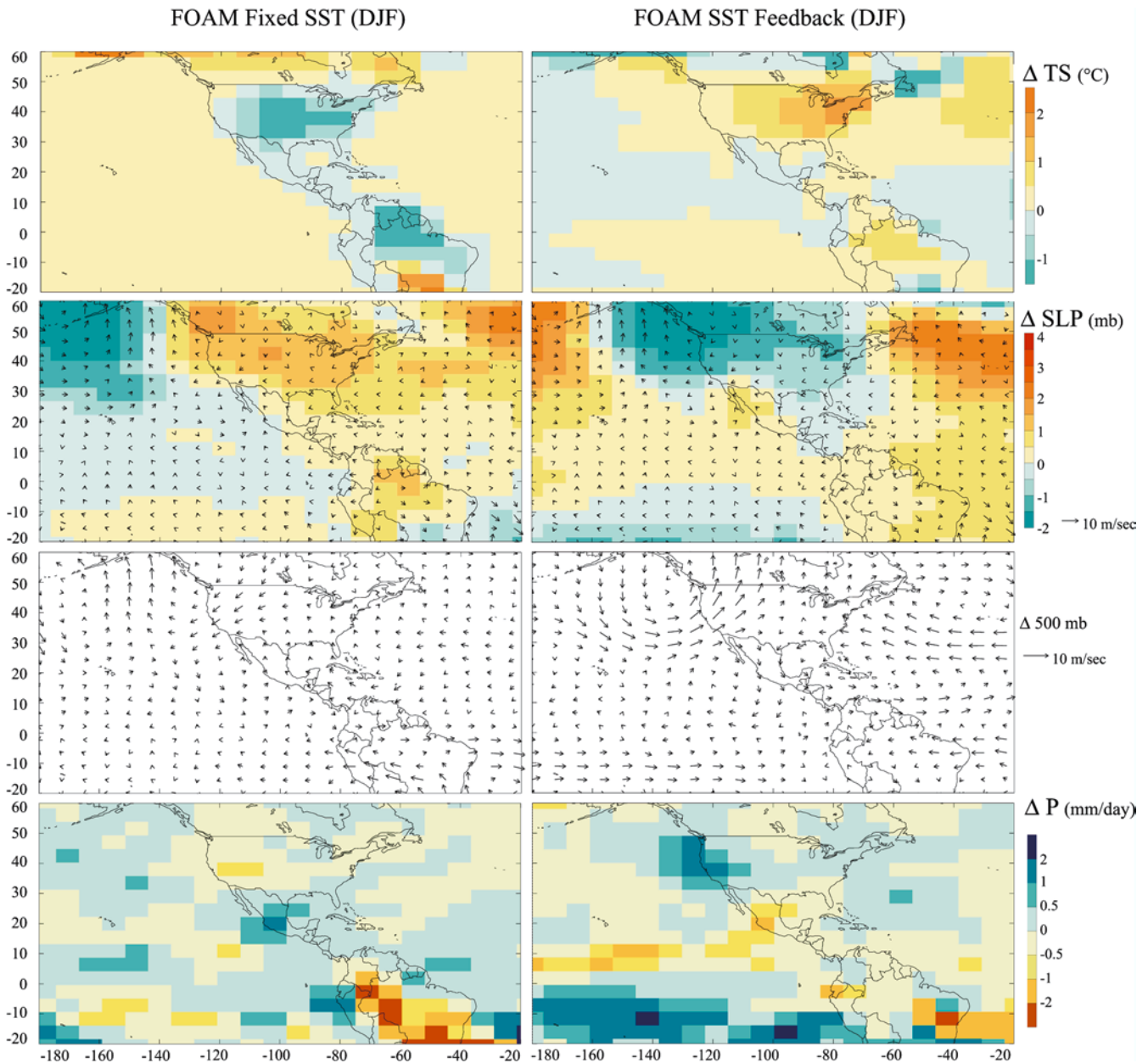

Fig. 8 Anomalies (6 ka minus 0 ka) of winter (December, January, February: DJF) surface temperature (*TS*), sea level pressure (*SLP*) and surface winds, 500 mb winds, and precipitation (*P*) from the FOAM (*left*) and CSM (*right*) coupled OAGCM simulations

eraged precipitation for the Pacific Northwest and mid-continental North America, and for the American West, shows no significant change between 6 ka and 0 ka (Table 5). There is a rather small increase (0.1 mm/day) in areally averaged precipitation over Central America, and a similarly small decrease (–0.1 mm/day) in northern South America.

The CSM (Fig. 8 right) has somewhat more enhanced cooling over the American continent (and also warming at high northern latitudes similar to FOAM). The temperature changes are generally not statistically significant north of 30°N. The CSM has enhanced pressure increases over land, a similarly intensified Aleutian low, intensified westerlies over the North Pacific at 30°N, and enhanced troughing over Central America near 15–20°N. Precipitation is likewise increased along the west coast, and across Central America, but slightly decreased over most of the interior of North America (not statistically significant). Overall, both models simulate similar responses to the decreased winter insolation.

The palaeoenvironmental changes implied by the vegetation, lake status and aeolian data do not allow us to address the realism of the simulated changes in winter precipitation. Although a few lake sites along the Gulf coast and in Florida appear to indicate wetter conditions than today, which is likely to reflect changes in winter precipitation regimes (Harrison et al. 2002) consistent with the simulated changes in precipitation, most of the sites in southeastern North America show no change in lake status compared to present. The observed vegetation changes in eastern North America are primarily driven by changes in temperature and are comparatively insensitive to the relatively small changes in moisture regimes implied by the simulations.

5.5 The role of direct radiative forcing over land on the mid-Holocene Northern Hemisphere winter (DJF) monsoon

The direct radiative effect of reduced wintertime insolation over land is that the continents become colder. In the FOAM simulation with fixed SSTs, this cooling occurs over northern hemisphere land south of about 50°N (Fig. 9, left panels). This cooling of the land leads to higher sea-level pressure, divergent near-surface outflow from the land toward the ocean, increased downward motion, and a drier continental interior. The cooling increases the low-level baroclinicity (in effect, an anomalous cold-core cyclone) which accounts for the increased westerlies over Central America and the decreased westerlies over the mid-continent. This southward-shift of the tropospheric westerlies and the storm track produces an enhancement of winter precipitation over Baja and Central America, the Gulf coast, and southeast Atlantic coast (Fig. 9, left panels). The changes along the Gulf coast and the southeast Atlantic coast are not statistically significant.

5.6 The role of SST feedback and the combined effects of direct radiation and SST feedbacks in the coupled atmosphere/ocean response of the mid-Holocene Northern Hemisphere winter (DJF) monsoon

The warmer eastern North Pacific, a part of the high-latitude wintertime response discussed elsewhere (Kutzbach and Gallimore 1988), is associated with an intensified Aleutian Low, warm air advection over the continent, and enhanced precipitation along the west coast, but decreased precipitation in Central America (Fig. 9 right). These changes partially cancel the changes due to direct radiative effects over land (Fig. 9 left). However, the combined impact of direct radiative forcing and ocean feedbacks (Fig. 8 left) produces increased precipitation along the west coast and, to a lesser extent, over Central America and the Gulf Coast. The results from a FOAM simulation for 11 k (Liu et al. 1999b) and a GENESIS simulation at 6 ka (Doherty et al. 2000) are similar enough to the FOAM and CSM simulations for 6 ka to suggest that these are robust responses to wintertime changes in insolation.

5.7 The response of the mid-Holocene Southern Hemisphere summer (DJF) monsoon to orbital forcing and SST feedbacks

Both models show very similar reductions in summertime (DJF) precipitation over South America south of the equator (Fig. 8). The strong role of direct radiative forcing over land in decreasing the strength of the Southern Hemisphere American summer monsoon is clear from the FOAM experiment with fixed SSTs (Fig. 9 left). SST feedbacks do not alter this response over most of the Amazon Basin. However, a slight southward shift of the south Atlantic ITCZ contributes to further precipitation decline near the coast (Fig. 9 right) although this feature is of marginal statistical significance. The placement of the south Atlantic ITCZ in the control simulation is rather poor (Liu et al. unpublished), and therefore the reliability of this feature of the response is uncertain because of the possible bias in model climatology.

There is insufficient data from the Amazon Basin to confirm the simulated changes. The limited amount of information from sites along the west coast and on the Andean Plateau (Fig. 3) is consistent with increased moisture availability. Thus, these data tend to confirm the simulated changes in precipitation.

5.8 Patterns of change in mean annual temperature and precipitation

The annual average temperature simulated by FOAM (Fig. 10 left) is slightly higher than today at 6 ka over most of North America, but slightly lower in the American Southwest (not statistically significant), Cen-

tral America and in northern South America. The pattern of change in annual average precipitation in FOAM (Fig. 10 left) is dominated by the JJA pattern. The DJF response augments the JJA response over Central America and the west coast of North America. However, along the Gulf Coast, the winter increase somewhat offsets the JJA decrease. The pattern of changes in mean annual temperature and precipitation in the CSM simulation (Fig. 10 right) are generally similar to FOAM. The simulated drying in the southeast is not as significant as in FOAM. The temperature changes in the CSM simulation are generally not statistically significant.

6 Discussion and conclusions

The study of Holocene climates with climate models has progressed from early studies with atmospheric general circulation models (AGCMS) with fixed SSTs (Kutzbach and Otto-Bliesner 1982; Kutzbach and Guetter 1986; Kutzbach et al. 1993; Joussaume et al. 1999), AGCMS coupled to mixed-layer oceans (Kutzbach and Gallimore 1998; Kutzbach et al. 1998) and most recently to studies with coupled dynamical models of atmosphere and ocean (Hewitt and Mitchell 1998; Otto-Bliesner 1999; Bush 1999; Liu et al. 1999b; Braconnot et al.

Fig. 9 Anomalies (6 ka minus 0 ka) of winter (December, January, February: DJF) surface temperature (*TS*), sea level pressure (*SLP*) and surface winds, 500 mb winds, and precipitation (*P*) from the FOAM simulation made with fixed (modern) sea-surface temper-atures and reflecting the direct response to orbital forcing over land (*left*) as compared with the SST feedback response (*right*), obtained by subtracting the results with fixed SSTs from the results of the fully-coupled FOAM simulation
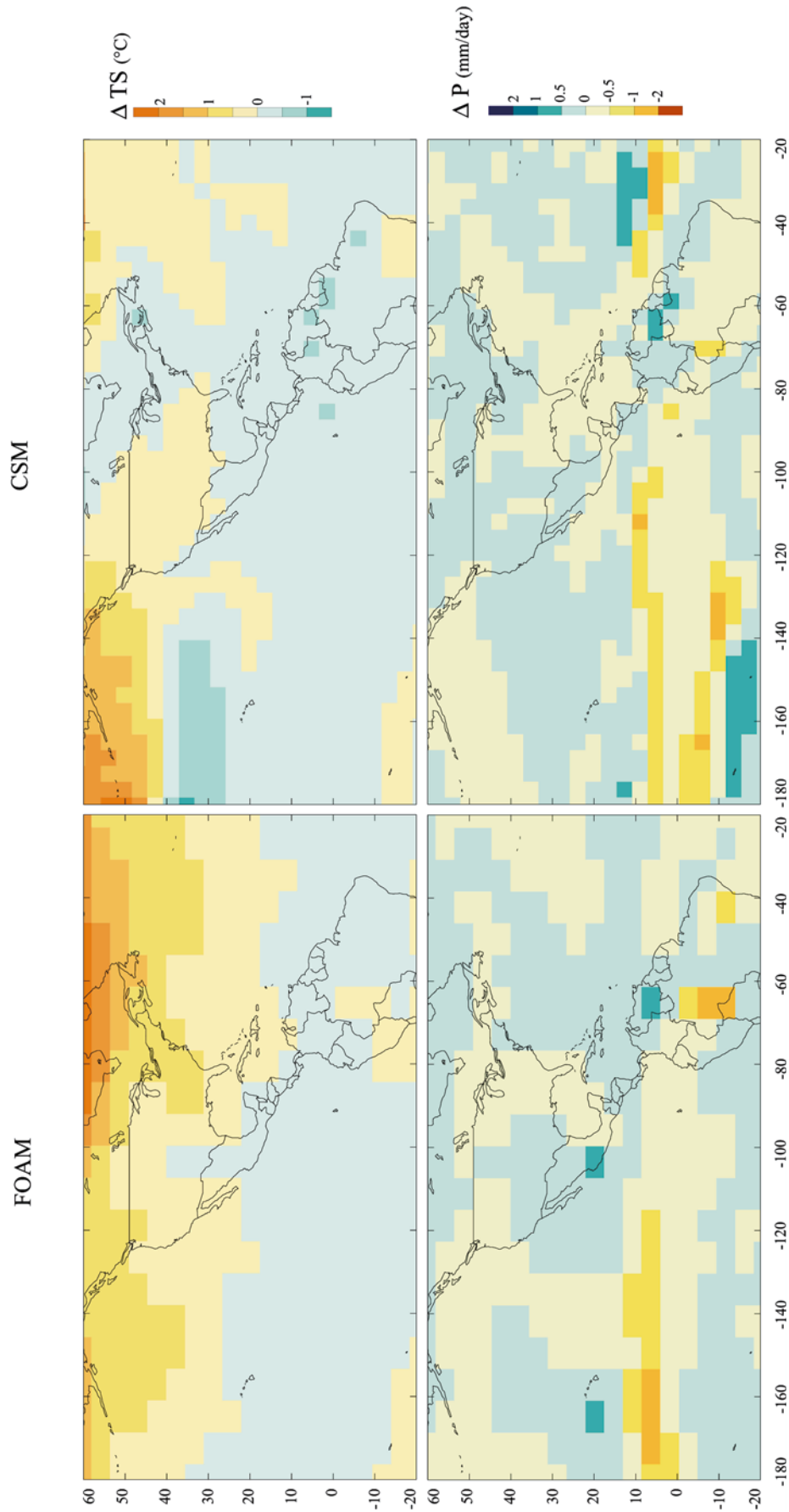
Fig. 10 Changes in annual average temperature (*TS*) and precipitation (*P*) for the two fully coupled simulations: FOAM (*left*) and CSM (*right*)

2000). The move toward models of increasing complexity has been driven to a large extent by the realization that atmosphere-only 6 ka simulations with fixed modern SSTs underestimate the observed response to orbital forcing (Yu and Harrison 1996; Harrison et al. 1998; Joussaume et al. 1999; Kohfeld and Harrison 2000; Harrison 2000).

The responses of FOAM and CSM are similar, suggesting that the dynamical features shown in these simulations are robust responses to 6 ka orbital forcing. In both FOAM and CSM, the North American response includes a distinctive pattern of wetter in the southwest and drier in most other areas. This response occurs because increased low-level convergence and upward motion in the core monsoon regions of Mexico and the American Southwest necessarily lead to the creation of a generally crescent-shaped area of enhanced subsidence bordering the region of enhanced precipitation. The model results thus provide a coherent dynamical explanation for regional patterns of increased or decreased aridity at 6 ka shown by palaeoenvironmental data from the Americas. This feature of the model's remote response to orbitally enhanced summer-monsoon precipitation is similar in structure, though different in spatial detail, to the modern climatological response to enhanced precipitation in the American Southwest derived from studies of interannual variability (Fig. 2, and Higgins et al. 1997, 1998). This similarity between the orbitally forced response and the internal-variability response indicates that dynamical processes help to define the spatial patterns of wet/dry anomalies in both cases.

The FOAM experiments show that SST feedbacks produce a much larger enhancement of precipitation in Central America than direct radiative forcing alone. Higgins and Shi (2000) attribute the precipitation increase over the American Southwest shown by modern data to a teleconnection from the colder equatorial Pacific. Furthermore, our analyses of the NCEP reanalysis data (Fig. 2) show that enhanced precipitation over Central America is accompanied by a northward shift of the ITCZ, enhanced southerlies, and cooler equatorial SSTs. Although ocean feedbacks have been shown to contribute significantly to the mid-Holocene enhancement of monsoons in other regions (e.g., Braconnot et al. 2000; Kutzbach et al. 2001), there are no other cases where the ocean feedback is the dominant cause of monsoonal enhancement (Liu et al. unpublished). In Africa, for example, SST feedback enhances the monsoon, but the feedback effect is only 50% (or less) of the direct radiative effect.

FOAM results show that the direct radiative response in winter produces a colder continent and a southward-shifted storm track. This response is only slightly modified by SST feedbacks. The southward-shifted storm track leads to increased winter precipitation along the west coast of North America, through Central America and along the Gulf Coast. Along the west coast and in Central America, the changes in winter augment the

increase in summer precipitation. The increased precipitation along the Gulf Coast offsets the simulated decrease in precipitation during the summer. Although the simulated changes are small compared to the changes occurring during summer, and affect only a relatively narrow coastal zone, they nevertheless suggest that changes in the winter monsoon may be important in explaining regional climate changes at 6 ka.

The same basic continental response to orbital forcing occurs in the Americas as in other northern continents, but the response is weaker because the North American continent is smaller. The SST feedback and northward shift of the ITCZ are similar to the mechanism described previously in explanations of the enhanced northern African monsoon during the mid-Holocene (Kutzbach and Liu 1997; Liu et al. 1999b). However, Liu et al. (1999a and unpublished) find rather different mechanisms for the Indian and East Asian monsoons.

The role of biogeophysical vegetation feedbacks is not considered here, but this has proven to be an important aspect of the African monsoon story, not only amplifying the response to orbital forcing but also lengthening the wet season (Texier et al. 1997; Ganopolski et al. 1998; Braconnot et al. 1999; Doherty et al. 2000; Kutzbach et al. 2001). Thus, we expect that vegetation feedbacks would produce a further enhancement of precipitation in the case of the northern American summer monsoon, and further reduction of precipitation in the case of the southern American summer monsoon. These possibilities will be addressed as fully coupled land–ocean–atmosphere models, currently under active development, become available for palaeoclimate simulations.

References

Adams DK, Comrie AC (1997) The North American monsoon. Bull Am Meteorol Soc 78: 2197–2213

Bonan GB (1998) The land surface climatology of the NCAR Land Surface Model coupled to the NCAR Community Climate Model. J Clim 11: 1307–1326

Boville BA, Gent PR (1998) The NCAR Climate System Model, Version 1. J Clim 11: 1115–1130

Boville BA, Hurrell JW (1998) A comparison of the atmospheric circulations simulated by the CCM3 and CSM1. J Clim 11: 1327–1341

Braconnot P, Joussaume S, Marti O, de Noblet N (1999) Synergistic feedbacks from ocean and vegetation on the African monsoon response to mid-Holocene insolation. Geophys Res Lett 26: 2481–2484

Braconnot P, Marti O, Joussaume S, Leclainche Y (2000) Ocean feedback in response to 6 kyr BP insolation. J Clim 13: 1537–1553

Broström A, Coe M, Harrison SP, Gallimore R, Kutzbach JE, Foley J, Prentice IC, Behling P (1998) Land surface feedbacks and palaeomonsoons in northern Africa. Geophys Res Lett 25: 3615–3618

Bryson RA, Lowry WP (1955) Synoptic climatology of the Arizona summer precipitation singularity. Bull Am Meteorol Soc 36: 329–339

Bush ABG (1999) Assessing the impact of mid-Holocene insolation on the atmosphere–ocean system. Geophys Res Lett 26: 99–102

Cheddadi R, Yu G, Guiot J, Harrison SP, Prentice IC (1997) The climate of Europe 6000 years ago. Clim Dyn 13: 1–9

Dean WE, Ahlbrandt TS, Anderson RY, Bradbury JP (1996) Regional aridity in North America during the middle Holocene. The Holocene 6: 145–155

Doherty R, Kutzbach JE, Foley J, Pollard D (2000) Fully-coupled climate/dynamical vegetation model simulations over northern Africa during the mid-Holocene. Clim Dyn 16: 561–573

Douglas MW, Maddox RA, Howard K, Reyes S (1993) The Mexican monsoon. J Clim 6: 1665–1677

Edwards ME, Anderson PM, Brubaker LB, Ager TA, Andreev AA, Bigelow NH, Cwynar LC, Eisner WR, Harrison SP, Hu FS, Jolly D, Lozhkin AV, McDonald GM, Mock CJ, Ritchie JC, Sher AV, Spear RW, Williams JW, Yu G (2000) Pollen-based biomes for Beringia 18,000, 6000 and 0 ^{14}C yr B.P. J Biogeogr 27: 521–554

Farrera I, Harrison SP, Prentice IC, Ramstein G, Guiot J, Bartlein PJ, Bonnefille R, Bush M, Cramer W, von Grafenstein U, Holmgren K, Hooghiemstra H, Hope G, Jolly D, Lauritzen SE, Ono Y, Pinot S, Stute M, Yu G (1999) Tropical palaeoclimates at the Last Glacial Maximum: a new synthesis of terrestrial data. I. Vegetation, lake-levels and geochemistry. Clim Dyn 15: 823–856

Fein JS, Stephens PL (eds) (1987) Monsoons. J Wiley, New York, pp 632

Feng ZD, Johnson WC, Lu YC, Ward PA (1994) Climatic signals from loess-soil sequences in the central Great-Plains, USA. Palaeogeogr Palaeoclim Palaeoecol 110: 345–358

Forman SL, Oglesby R, Markgraf V, Stafford T (1995) Paleoclimatic significance of Late Quaternary eolian deposition on the Piedmont and High-Plains, Central United-States. Glob Planet Change 11: 35–55

Forman SL, Oglesby R, Webb RS (2001) Temporal and spatial patterns of Holocene dune activity on the Great Plains of North America: megadroughts and climate links. Glob Planet Change 29: 1–29

Gajewski K, Gignac LD, Halsey L, John J, Maisongrande P, Mandell P, Mudie PJ, Richard PJH, Sherin AG, Soroko J, Vitt DH, Vance R, Sawada M, Fung I (2000) The climate of North America and adjacent oceans waters ca. 6 ka. Can J Earth Sci 37: 661–681

Ganopolski A, Kubatzki C, Claussen M, Brovkin V, Petoukhov V (1998) The influence of vegetation-atmosphere–ocean interaction on climate during the mid-Holocene. Science 280: 1916–1919

Gent PR, Bryan FO, Danabasoglu G, Doney SC, Holland WR, Large WG, McWilliams JC (1998) The NCAR Climate System Model global ocean component. J Clim 11: 1287–1306

Harrison SP (1989) Lake levels and climatic change in eastern North America. Clim Dyn 3: 157–167

Harrison SP (2000) Palaeoenvironmental data sets and model evaluation in PMIP. In: Braconnot P (ed) Modelling Intercomparison Project (PMIP). Proc Third PMIP Workshop, Canada, 4–8 October 1999. WCRP-111, WMO/TD-No. 1007, pp 25–42

Harrison SP, Yu G, Tarasov PE (1996) The Late Quaternary lake-level record from northern Eurasia. Quat Res 45: 138–159

Harrison SP, Jolly D, Laarif F, Abe-Ouchi A, Dong B, Herterich K, Hewitt C, Joussaume S, Kutzbach JE, Mitchell J, de Noblet N, Valdes P (1998) Intercomparison of simulated global vegetation distribution in response to 6 kyr B.P. orbital forcing. J Clim 11: 2721–2742

Harrison SP, Yu G, Vassiljev J (2002) Climate changes during the Holocene recorded by lakes from Europe. In: Wefer G, Berger WH, Behre K-E, Jansen E (eds) Climate development and history of the North Atlantic realm. Springer, Berlin Heidelberg, pp 191–204

Hastenrath S (ed) (1985) Climate and circulation of the tropics. Reidel Publishing, Dordrecht, pp 455

Hastenrath S (1990) Diagnostics and prediction of anomalous river discharge in Northern South-America. J Clim 3: 1080–1096

Hewitt CD, Mitchell JFB (1998) A fully coupled GCM simulation of the climate of the mid-Holocene. Geophys Res Lett 25: 361–364

Higgins RW, Shi W (2000) Dominant factors responsible for interannual variability of the summer monsoon in the southwestern United States. J Clim 13: 759–776

Higgins RW, Yao Y, Wang XL (1997) Influence of the North American monsoon system on the US summer precipitation regime. J Clim 10: 2600–2622

Higgins RW, Mo KC, Yao Y (1998) Interannual variability of the US summer precipitation regime with emphasis on the southwestern monsoon. J Clim 11: 2582–2606

Holliday VT (1997) Origin and evolution of lunettes on the high plains of Texas and New Mexico. Quat Res 47: 54–69

Hoskins B (1996) On the existence and strength of the summer subtropical anticyclones: the Bernard Haurwitz Memorial Lecture. Bull Am Meteorol Soc 77: 1287–1292

Jacob RL (1997) Low frequency variability in a simulated atmosphere ocean system. PhD thesis, University of Wisconsin-Madison, pp 170

Joussaume S, Braconnot P (1997) Sensitivity of paleoclimate simulation results to season definitions. J Geophys Res Atmos 102: 1943–1956

Joussaume S, Taylor KE, Braconnot P, Mitchell JFB, Kutzbach JE, Harrison SP, Prentice IC, Broccoli AJ, Abe-Ouchi A, Bartlein PJ, Bonfils C, Dong B, Guiot J, Herterich K, Hewitt CD, Jolly D, Kim JW, Kislov A, Kitoh A, Loutre MF, Masson V, McAvaney B, McFarlane N, de Noblet N, Peltier WR, Peterschmitt JY, Pollard D, Rind D, Royer JF, Schlesinger ME, Syktus J, Thompson S, Valdes P, Vettoretti G, Webb RS, Wyputta U (1999) Monsoon changes for 6000 years ago: results of 18 simulations from the Paleoclimate Modeling Intercomparison Project (PMIP). Geophys Res Lett 26: 859–862

Keen KL, Shane LCK (1990) A continuous record of Holocene eolian activity and vegetation change at Lake Ann, East-Central Minnesota. Geol Soc Am Bull 102: 1646–1657

Kiehl JT, Boville B, Briegleb B, Hack J, Rasch P, Williamson D (1996) Description of the NCAR Community Climate Model (CCM3). National Center for Atmospheric Research, Boulder, Colorado, pp 152

Kistler R, Kalnay E, Collins W, Saha S, White G, Woollen J, Chelliah M, Ebisuzaki W, Kanamitsu M, Kousky V, van den Dool H, Jenne R, Fiorino M (2001) NCEP-NCAR 50-year reanalysis: monthly means CD-ROM and documentation. Bull Am Meteorol Soc 82: 247–268

Kohfeld KE, Harrison SP (2000) How well can we simulate past climates? Evaluating the models using global palaeoenvironmental data sets. Quat Sci Rev 19: 321–346

Kutzbach JE, Gallimore RG (1988) Sensitivity of a coupled atmosphere mixed layer ocean model to changes in orbital forcing at 9000 years B.P. J Geophys Res 93: 803–821

Kutzbach JE, Guetter PJ (1986) The influence of changing orbital parameters and surface boundary conditions on climate simulations for the past 18000 years. J Atmos Sci 43: 1726–1759

Kutzbach JE, Liu Z (1997) Response of the African monsoon to orbital forcing and ocean feedbacks in the middle Holocene. Science 278: 440–443

Kutzbach JE, Otto-Bliesner BL (1982) The sensitivity of the African-Asian monsoonal climate to orbital parameter changes for 9000 years B.P. in a low-resolution general circulation model. J Atmos Sci 39: 1177–1188

Kutzbach JE, Webb III T (1993) Conceptual basis for understanding late-quaternary climates. In: Wright Jr HE, Kutzbach JE, Webb III T, Ruddiman WF, Street-Perrott FA, Bartlein PJ (eds) Global climates since the Last Glacial Maximum. University of Minnesota Press, Minneapolis, pp 5–11

Kutzbach JE, Guetter PJ, Behling PJ, Selin R (1993) Simulated climatic changes: results of the COHMAP climate-model experiments. In: Wright Jr HE, Kutzbach JE, Webb III T, Ruddiman WF, Street-Perrott FA, Bartlein PJ (eds) Global climates since the Last Glacial Maximum. University of Minnesota Press, Minneapolis, pp 24–93

Kutzbach JE, Gallimore R, Harrison SP, Behling P, Selin R, Laarif F (1998) Climate and biome simulations for the past 21,000 years. Quat Sci Rev 17: 473–506

Kutzbach JE, Harrison SP, Coe MT (2001) Land–ocean–atmosphere interactions and monsoon climate change: a palaeoperspective. In: Schulze ED, Heimann M, Harrison SP, Holland E, Lloyd J, Prentice IC, Schimel D (eds) Global biogeochemical cycles in the climate system. Academic Press, San Diego, pp 73–83

Liu Z, Gallimore RG, Kutzbach JE, Xu W, Golubev Y, Behling P, Selin R (1999a) Modeling long-term climate changes with equilibrium asynchronous coupling. Clim Dyn 15: 325–340

Liu Z, Jacob R, Kutzbach J, Harrison S, Anderson J (1999b) Monsoon impact on El Niño in the early Holocene. Pages Newsl 7: 16–17

Liu ZY, Kutzbach JE, Wu LX (2000) Modeling climatic shift of El Niño variability in the Holocene. Geophys Res Lett 27: 2265–2268

Liu Z, Wu L (2000) Tropical atlantic variability in a coupled GCM. Atmos Sci Lett 1: 26–36 (http://www.idealibrary.com/links/toc/asle/1/1/0)

Liu Z, Wu L, Gallimore R, Jacob R (2002) Search for the origins of Pacific decadal variability. Geophys Res Lett 29: DOI 10.1029/2001GL013735

Markgraf V, Baumgartner TR, Bradbury JP, Diaz HF, Dunbar RB, Luckman BH, Seltzer GO, Swetnam TW, Villalba R (2000) Paleoclimate reconstruction along the Pole-Equator-Pole transect of the Americas (PEP 1). Quat Sci Rev 19: 125–140

Metcalfe SE, O'Hara SL, Caballero M, Davies SJ (2000) Records of Late Pleistocene-Holocene climatic change in Mexico – a review. Quat Sci Rev 19: 699–721

Mitchell JFB, Grahame, NS, Needham, KJ (1988) Climate simulations for 9000 years before present: seasonal variations and the effect of the Laurentide Ice Sheet. J Geophys Res Atmos 93: 8283–8303

Mock CJ, Brunelle-Daines AR (1999) A modern analogue of western United States summer palaeoclimate at 6000 years before present. The Holocene 9: 541–545

Montoya M, Crowley TJ, von Storch H (1998) Temperatures at the last interglacial simulated by a coupled ocean–atmosphere climate model. Paleoceanogr 13: 170–177

Montoya M, von Storch H, Crowley TJ (2000) Climate simulation for 125 kyr BP with a coupled ocean–atmosphere general circulation model. J Clim 13: 1057–1072

Muhs DR, Zárate M (2001) Late Quaternary eolian records of the Americas and their paleoclimatic significance. In: Markgraf V (ed) Interhemispheric climate linkages. Academic Press, San Diego, pp 183–216

Otto-Bliesner BL (1999) El Niño, La Niña and Sahel precipitation during the middle Holocene. Geophys Res Lett 26: 87–90

Peterson TC, Vose RS (1999) Data Documentation for Data Set TD9100, Global Historical Climatology Network. National Climatic Data Center, Asheville, NC, pp 29 (htpp://www.ncdc.noaa.gov/pub/data/documentlibrary/tddoc/td9100.txt)

Prentice IC, Webb III T (1998) BIOME 6000: reconstructing global mid-Holocene vegetation patterns from palaeoecological records. J Biogeogr 25: 997–1005

Prentice IC, Guiot J, Harrison SP (1992) Mediterranean vegetation, lake levels and palaeoclimate at the Last Glacial Maximum. Nature 360: 658–660

Prentice IC, Jolly D, BIOME 6000 Members (2000) Mid-Holocene and glacial-maximum vegetation geography of the northern continents and Africa. J Biogeogr 27: 507–519

Ramage CS (ed) (1971) Monsoon meteorology. Academic Press, New York, pp 295

Rasmusson EM, Arkin PA (1993) A global view of large-scale precipitation variability. J Clim 6: 1495–1522

Ritchie JC, Harrison SP (1993) Vegetation, lake level, and climate in Western Canada during the Holocene. In: Wright Jr HE, Kutzbach JE, Webb III T, Ruddiman WF, Street-Perrott FA, Bartlein PJ (eds) Global climates since the Last Glacial Maximum. University of Minnesota Press, Minneapolis, pp 401–414

Rodwell MJ, Hoskins BJ (1996) Monsoons and the dynamics of deserts. Q J R Meteorol Soc 122: 1385–1404

Rodwell MJ, Hoskins BJ (2001) Subtropical anticyclones and summer monsoons. J Clim 14: 3192–3211

Stuiver M, Reimer PJ (1993) Extended ^{14}C data base and revised Calib 3.0 ^{14}C age calibration program. Radiocarbon 35: 215–230

Tang M, Reiter ER (1984) Plateau monsoons of the Northern Hemisphere: a comparison between North America and Tibet. Mon Weather Rev 112: 617–637

Texier D, de Noblet N, Harrison SP, Haxeltine A, Jolly D, Joussaume S, Laarif F, Prentice IC, Tarasov PE (1997) Quantifying the role of biosphere–atmosphere feedbacks in climate change: coupled model simulation for 6000 years BP and comparison with palaeodata for northern Eurasia and northern Africa. Clim Dyn 13: 865–882

Thompson RS, Anderson KH (2000) Biomes of western North America at 18,000, 6000, and 0 ^{14}C yr B.P. reconstructed from pollen and packrat midden data. J Biogeogr 27: 555–584

Thompson RS, Whitlock C, Bartlein PJ, Harrison SP, Spaulding WG (1993) Climatic changes in the western United States since 18,000 yr BP. In: Wright Jr HE, Kutzbach JE, Webb III T, Ruddiman WF, Street-Perrott FA, Bartlein PJ (eds) Global climates since the Last Glacial Maximum. University of Minnesota Press, Minneapolis, pp 468–513

Weatherly JW, Briegleb BP, Large WG, Maslanik JA (1998) Sea ice and polar climate in the NCAR CSM. J Clim 11: 1472–1486

Webb III T, Bartlein PJ, Harrison SP, Anderson KH (1993) Vegetation, lake-levels, and climate in eastern North America for past 18,000 years. In: Wright Jr HE, Kutzbach JE, Webb III T, Ruddiman WF, Street-Perrott FA, Bartlein PJ (eds) Global climates since the Last Glacial Maximum. University of Minnesota Press, Minneapolis, pp 415–467

Webster PJ (1987) The elementary monsoon. In: Fein JS, Stephens PI (eds) Monsoons. J Wiley, New York, pp 3–32

Williams JW, Webb III T, Richard PH, Newby P (2000) Late Quaternary biomes of Canada and the eastern United States. J Biogeogr 27: 585–607

Yu G, Harrison SP (1995) Lake status records from Europe: data base documentation. NOAA Paleoclimatology Publications Series Rep 3: 1–451

Yu G, Harrison SP (1996) An evaluation of the simulated water balance of Eurasia and northern Africa at 6000 y BP using lake status data. Clim Dyn 12: 723–735

Zhou JY, Lau KM (1998) Does a monsoon climate exist over South America? J Clim 11: 1020–1040